Journal of
Medicinal Chemistry

Article

Discovery of first in vivo active inhibitors of soluble epoxide hydrolase (sEH) phosphatase domain

Jan S Kramer, Stefano Woltersdorf, Thomas Duflot, Kerstin Hiesinger, Felix F Lillich, Felix Knöll, Sandra K Wittmann, Franca M Klingler, Steffen Brunst, Apirat Chaikuad, Christophe Morisseau, Bruce D. Hammock, Carola Buccellati, Angelo Sala, G. Enrico Rovati, Matthieu Leuillier, Sylvain Fraineau, Julie Rondeaux, Victor Hernandez Olmos, Jan Heering, Daniel Merk, Denys Pogoryelov, Dieter Steinhilber, Stefan Knapp, Jeremy Bellien, and Ewgenij Proschak

J. Med. Chem., **Just Accepted Manuscript** • DOI: 10.1021/acs.jmedchem.9b00445 • Publication Date (Web): 22 Aug 2019

Just Accepted

is published by the American Chemical Society. 1155 Sixteenth Street N.W., Washington, DC 20036

	Chemistry Bellien, Jeremy; University Hospital Centre Rouen Proschak, Ewgenij; Goethe-Universitat Frankfurt am Main, Institute of Pharmaceutical Chemistry

Discovery of first in vivo active inhibitors of soluble epoxide hydrolase (sEH) phosphatase domain

Jan S. Kramer[1‡], Stefano Woltersdorf[1‡], Thomas Duflot[2], Kerstin Hiesinger[1], Felix F. Lillich[1], Felix Knöll[1], Sandra K. Wittmann[1], Franca-M. Klingler[1], Steffen Brunst[1], Apirat Chaikuad[1,3], Christophe Morisseau[4], Bruce D. Hammock[4], Carola Buccellati[5], Angelo Sala[5], G. Enrico Rovati[5], Matthieu Leuillier[6], Sylvain Fraineau[6], Julie Rondeaux[6], Victor Hernandez Olmos[1,7], Jan Heering[1,7], Daniel Merk[1], Denys Pogoryelov[8], Dieter Steinhilber[1], Stefan Knapp[1,2], Jeremy Bellien[6,9], and Ewgenij Proschak[1,]*

[1] Institute of Pharmaceutical Chemistry, Goethe-University Frankfurt, Max-von-Laue-Strasse 9, 60438 Frankfurt a. M., Germany.

[2] Laboratory of Pharmacokinetics, Toxicology and Pharmacogenetics, Rouen University Hospital, 76000 Rouen, France

[3] Structural Genomics Consortium, Buchmann Institute for Life Sciences, Goethe-University Frankfurt, Max-von-Laue-Strasse 15, 60438 Frankfurt a. M., Germany.

[4] Department of Entomology and Nematology, and UC Davis Comprehensive Cancer Center, University of California Davis, 95616 Davis, USA.

[5] Department of Pharmacological and Biomolecular Sciences, University of Milan, Via Balzaretti, 9, 20133, Milan, Italy

[6] Normandie Univ, UNIROUEN, INSERM U1096, 1 rue de Germont, 76000 Rouen, France

[7] Fraunhofer IME-TMP, Max-von-Laue-Strase 9, 60438 Frankfurt a. M., Germany

[8] Institute of Biochemistry, Goethe-University Frankfurt, Max-von-Laue-Strasse 9, 60438 Frankfurt a. M., Germany.

[9] Department of Clinical Pharmacology, Rouen University Hospital, 76000 Rouen, France

KEYWORDS

soluble epoxide hydrolase, phosphatase, oxazoles, crystal structure, chemical probe, lysophosphatidic acid

ABSTRACT

The emerging pharmacological target soluble epoxide hydrolase (sEH) is a bifunctional enzyme exhibiting two different catalytic activities, which are located in two distinct domains. Although the physiological role of the C-terminal hydrolase domain is well-investigated, little is known about its phosphatase activity located in the N-terminal domain of the sEH (sEH-P). Herein, we report the discovery and optimization of the first inhibitor of human and rat sEH-P, applicable in vivo. X-ray structure analysis of the sEH phosphatase domain complexed with an inhibitor provides insights in the molecular basis of small-molecule sEH-P inhibition and helps to rationalize the structure-activity relationships. 4-(4-(3,4-Dichlorophenyl)-5-phenyloxazol-2-yl)butanoic acid **(22b,** SWE101**)** has an excellent pharmacokinetic and pharmacodynamic profile in rats and enables the investigation of the physiological and pathophysiological role of sEH-P in vivo.

Introduction

The homodimeric soluble epoxide hydrolase (sEH) consists of two functionally different domains which are connected by a flexible proline-rich linker[1]. The C-terminal domain catalyzes the conversion of epoxyeicosatrienoic acids (EETs) and related epoxy fatty acids (EpFAs) towards the corresponding α,β-diols. The role of this hydrolase activity of sEH is well studied, and inhibitors of the C-terminal domain (sEHI) hold promising therapeutical potential in various diseases including diabetes, fibrosis, chronic pain, cardiovascular and neurodegenerative diseases[2]. The very broad therapeutical scope of sEHI is based on the hypothesis that while an accumulation of EpFAs has no or little effect under physiological conditions, they can prevent mitochondrial dysfunction and reduce subsequent reactive oxygen species (ROS) formation and the endoplasmic reticulum stress conditions[3]. Accordingly, sEHI targeting the hydrolase domain are in the focus of drug discovery and two candidates have already reached clinical development[2,4].

In contrast to the well-understood function of the C-terminal hydrolase domain, the role of the N-terminal phosphatase domain remains unclear. In 2003, Cronin et al.[5] and Newman et al.[6] independently reported a phosphatase activity of the N-terminal domain of the sEH (sEH-P). In vitro, sEH-P is able to hydrolyze diverse lipid phosphates including farnesyl pyrophosphate[7], sphingosine-1-phosphate, and lysophosphatidic acid[8,9]. The mechanism of lipid phosphate hydrolysis is well-investigated[10]. However, neither the endogenous substrate nor its physiological and possibly pathophysiological role have been identified so far[11]. Several molecules with sEH-P inhibitory activity have been identified up to date. Sodium dodecyl sulfate (**1**, SDS)[7] and *N*-acetyl-*S*-farnesyl-L-cysteine (**2**)[12,13] are lipid-like inhibitors of sEH-P. SMTP-7 (**3**), an investigational thrombolytic drug for treatment of ischemic stroke that simultaneously

inhibits both, the hydrolase and phosphatase activities of sEH[14]. The development of high-throughput screening assays for sEH-P led to discovery of ebselen (**4**)[15] and oxaprozin (**5**)[16] as novel sEH-P inhibitors. While **4** also affects sEH hydrolase activity, **5** is a selective but weak inhibitor of sEH-P (IC_{50} = 5 μM). In this study, we investigate the structure-activity relationships (SAR) of oxazole-based sEH-P inhibitors using the non-steroidal anti-rheumatic drug **5** as a starting point.

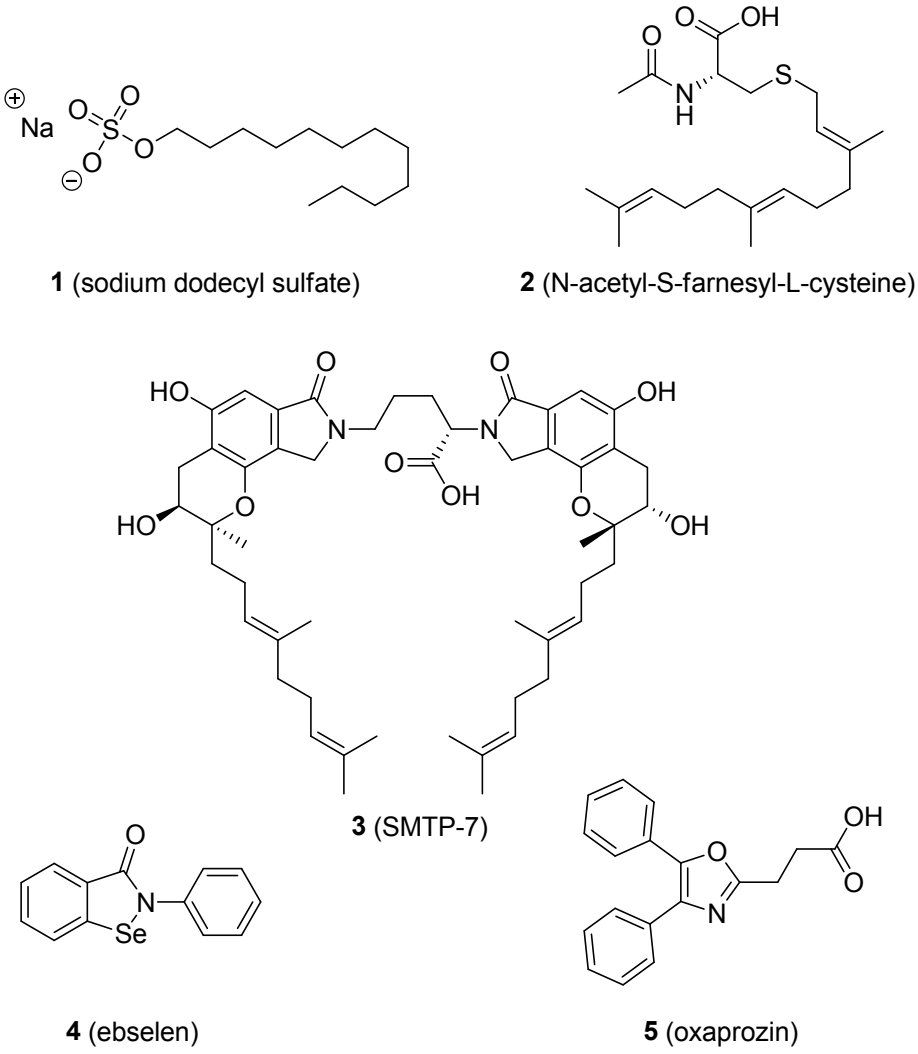

1 (sodium dodecyl sulfate) **2** (N-acetyl-S-farnesyl-L-cysteine)

3 (SMTP-7)

4 (ebselen) **5** (oxaprozin)

Figure 1. Structures of previously identified inhibitors of sEH-P activity **1-5**

Results and Discussion

Chemistry

The 2,4,5-trisubstituted oxazole scaffold of compound **5** is accessible via Blümelein-Lewy synthesis or starting from α-acyloxy ketones. In both methods, α-bromo-deoxybenzoins or benzoin derivatives can be employed as starting materials to generate the heterocycle. However, crossed benzoin derivatives with two different aryl moieties are not easily accessible whereas, asymmetric deoxybenzoins can be obtained from O-protected cyanohydrins as reported by Stork et al.[17] which are subsequently converted into α-bromo-ketones. This approach allows a very flexible alteration of the oxazole scaffold in all three substituent positions and enables a comprehensive structure-activity relationship analysis.

To investigate the importance of the carbon in the alkyl linker of **5**, thioglycolic acid derivative **9** was synthesized in two steps from 4,5-diphenyloxazole-2-thiol **6** and methyl 2-bromoacetate **7** resulting in methyl ester **8** which was subsequently hydrolysed (**Scheme 1**).

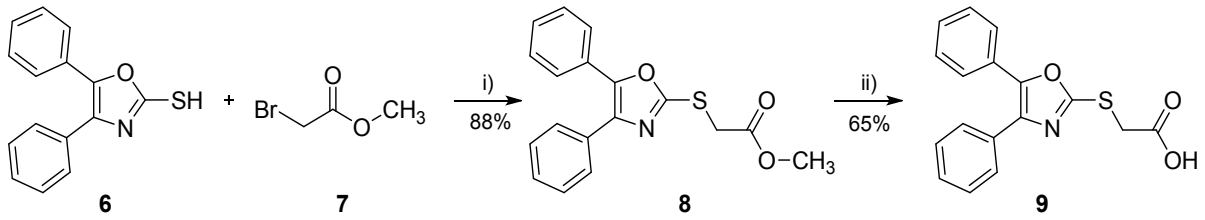

Scheme 1: i) Et_3N, THF, rt, 24 h; ii) KOH, MeOH/H_2O/THF, 70 °C, 15 min μw.

Amide derivative **12** was obtained from commercially available α-bromo-deoxybenzoin **10** and succinic amide **11** reacting under basic conditions to an α-acyloxy ketone which under heating in acetic acid in presence of excess of ammonium acetate cyclized to the oxazole **12 (Scheme 2)**.

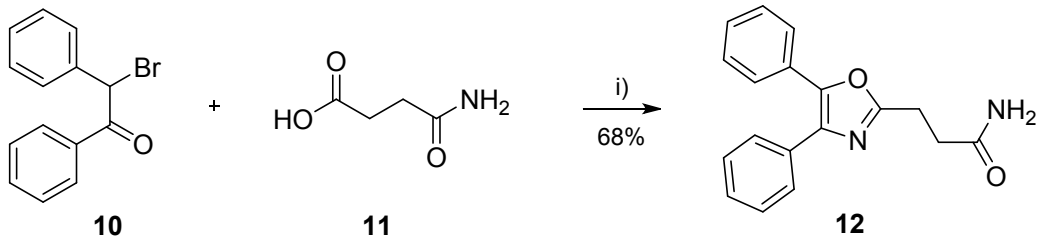

Scheme 2: i) 1. Et_3N, acetonitrile, 45°C, 6 h; 2. NH_4OAc, AcOH, reflux, 3 h.

Synthesis of oxaprozin derivatives **20a-m**, with alterations in the 4-phenyl moiety of the oxazole core structure, started from benzaldehydes **13a-m** as shown in **Scheme 3**. The substitution strategy followed the Topliss optimization scheme[18]. Benzaldehydes **13a-m** were treated with trimethylsilyl cyanide (TMSCN, **14**) in the presence of catalytic amounts of triethylamine under neat conditions to yield silyl protected cyanohydrins **15a-m**. As described by Stork et al.[17] *O*-protected cyanohydrins are easily deprotonated in α-position by LDA in THF, obtaining a stable nucleophile at low temperatures, which can react with an electrophile, in this case benzyl bromide **16**. The desired deoxybenzoins **17a-m** were subsequently obtained by cleaving the remaining silyl ether group of the intermediate with tetrabutylammonium fluoride solution (TBAF). Deoxybenzoins derivatives **17a-m** were then transformed to the appropriate α-bromo-deoxybenzoins **18a-m** under heating with bromine in dichloromethane. The respective α-bromo-deoxybenzoins **18a-m** were subsequently reacted with succinic acid **19** under basic conditions to α-acyloxy ketones which under heating in acetic acid and in presence of excess of ammonium acetate yielded oxaprozin derivatives **20a-m**.

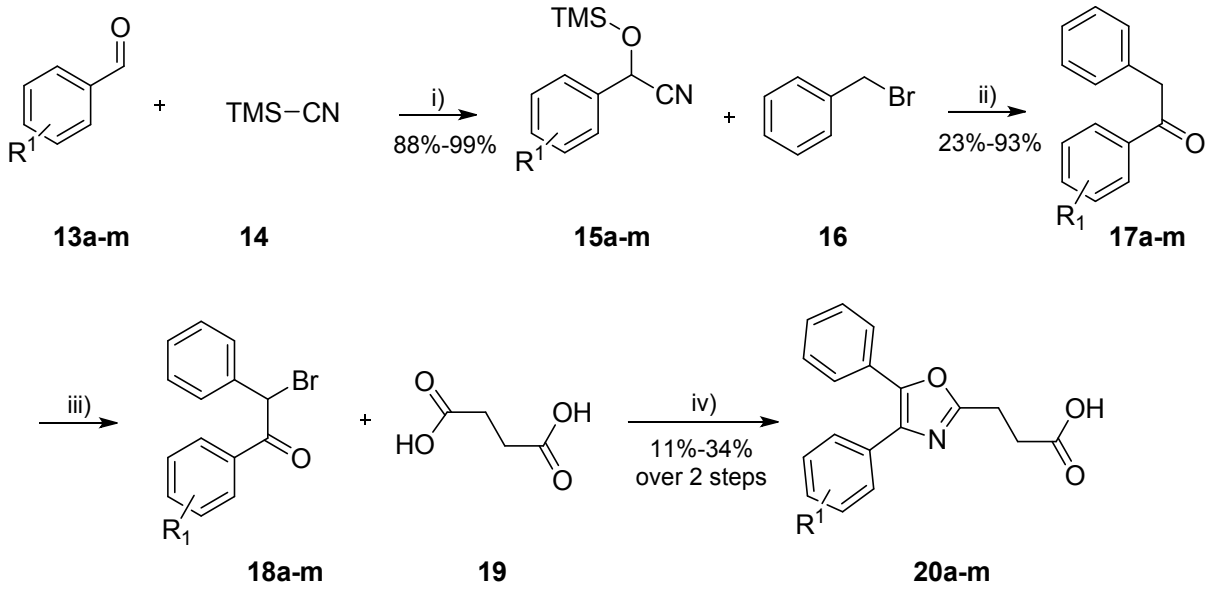

Scheme 3: i) Et_3N, 24 h; ii) 1. LDA, THF, -78°C→rt, 24 h; 2. TBAF, 30 min; iii) Br_2, $CHCl_3$, reflux, 2 h; iv) 1. Et_3N, MeCN, 45°C, 6 h; 2. NH_4OAc, AcOH, reflux, 3 h.

Synthesis of oxaprozin derivatives **22a-e**, with alterations in the oxazole 2-substituent is depicted in **Scheme 4**. Starting from intermediate **18l**, **22a-e** were obtained by the same strategy as described above for oxaprozin derivatives **20a-m** using dicarboxylic acids **21a-e** with different length and rigidity.

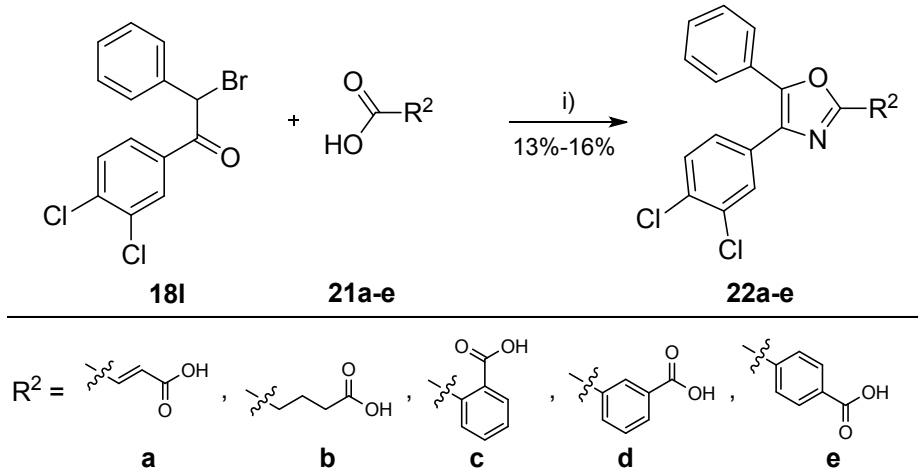

Scheme 4: i) 1. dicarboxylic acid **21a-e**, Et_3N, MeCN, 45°C, 6h; 2. NH_4OAc, AcOH, reflux 3h.

For alteration of the 5-phenyl moiety of the oxazole ring, a different synthetic approach was chosen to reduce the synthetic efforts. The adjusted strategy (**Scheme 5**) employed 3,4-dichlorophenylacylbromide **23** and glutaric acid **21b** to obtain α-acyloxy ketone **24** under basic conditions which reacted under heating in BF_3*Et_2O and in presence of excess acetamide to oxazole **25**. The oxazole 5-position was then activated for following Suzuki-cross-coupling by introduction of bromine with NBS in acetonitrile yielding key intermediate **26** for final modification. Coupling of **26** to oxaprozin derivatives **28a-k** with the appropriate boronic acid derivatives **27a-k** succeeded in DMF/water with tetrakis-(triphenylphosphine)-palladium(0) as catalyst and potassium phosphate as base.

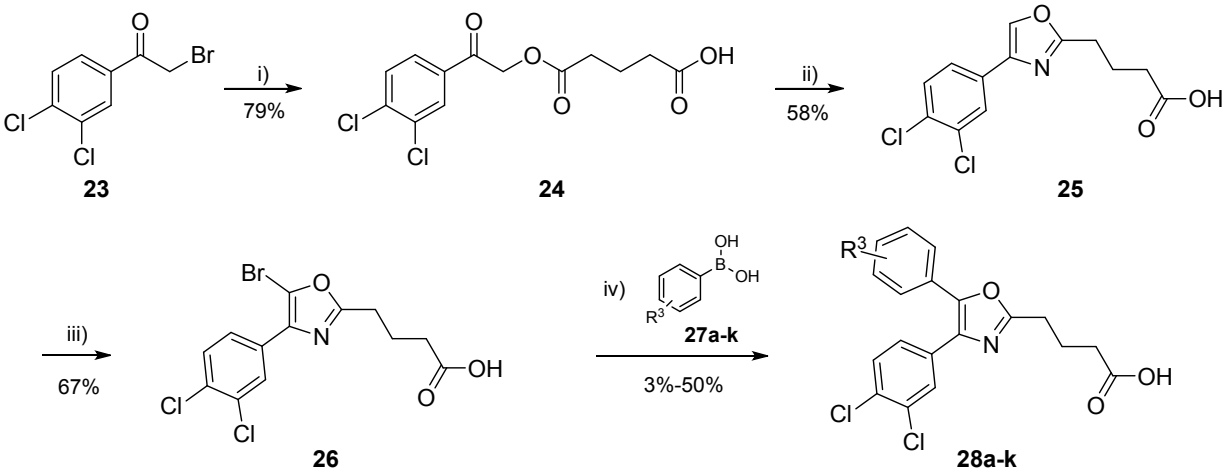

Scheme 5: i) glutaric acid **21b**, Et_3N, acetone, TLC-control; ii) acetamide, BF_3*Et_2O, 140 °C, 30 h; iii) NH_4OAc, NBS, acetonitrile, rt, 1.5 h; iv) boronic acid derivative **27a-k**, K_3PO_4, DMF/H_2O 2/1, $Pd(PPh_3)_4$, 55-80 °C, 30-48 h.

Structure-activity relationships

The exploration of structure-activity relationships of substituted oxazoles was performed using a fluorescence-based enzyme activity assay as reported previously[16]. In this kinetic assay, the conversion of the fluorogenic substrate fluorescein diphosphate by the recombinant sEH-P domain is monitored to assess the inhibitory potency of the test compounds. Bioisosteric replacement of the β-methylene bridge by sulfur (**9**) slightly diminished potency while replacement of the carboxylate by a primary amide (**12**) resulted in complete loss of activity. Replacement of the oxazole core in pyrazole **29** was also not tolerated (**Figure 2**).

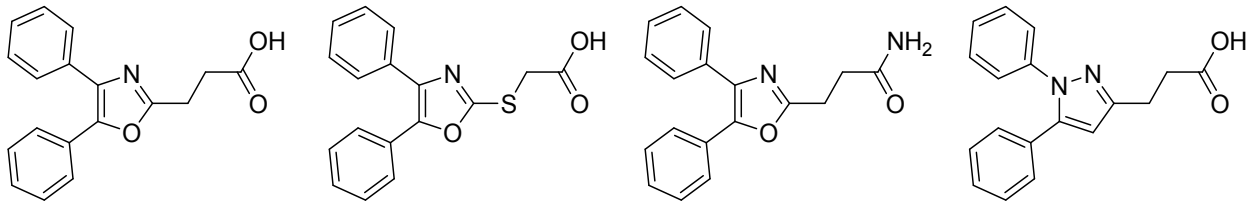

5 IC_{50} = 5 µM

9 IC_{50} = 17 µM

12 inactive

29 IC_{50} > 50 µM

Figure 2. Initial diversification of **5**.

The next optimization round addressed the 4-position of the oxazole ring (**Table 1**). *Ortho*-substituted phenyl moieties as they were present in compounds **20a** and **20b** were poorly tolerated, while meta substituted phenyl residues (**20c** and **20d**) retained similar potency as **5**. The SAR of *para* substituted phenyl residues in the 4-position of the oxazole core was more sophisticated. While fluorine (**20e**) only slightly diminished the potency, larger electron-withdrawing moieties such as trifluoromethyl (**20f**) or nitrile (**20g**) led to a loss of activity. A

chlorine substituent at this position (**20h**) slightly enhanced inhibitory potency while the electron-releasing methoxy moiety (**20i**) decreased activity. Following the Topliss optimization scheme[18], a second chlorine substituent was introduced in the meta-position of the phenyl ring (**20k**) which led to a more than tenfold increase in sEH-P inhibition. Other variants of the chlorine substitution pattern (**20l** and **20m**) did not lead to potency improvement.

Table 1. Optimization of the 4-position of the oxazole core.

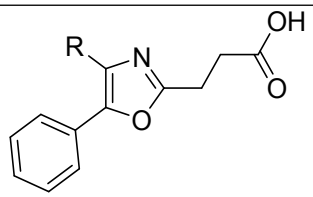

Cpd	R	IC_{50} [μM]	**Cpd**	R	IC_{50} [μM]
5	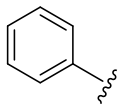	5 ± 1	**20g**	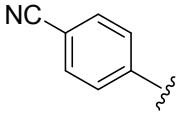	44 ± 5
20a	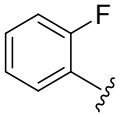	40 ± 12	**20h**	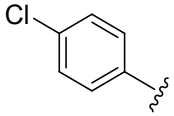	3 ± 1
20b	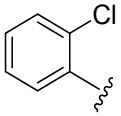	33 ± 7	**20i**	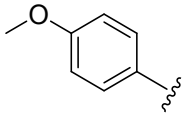	18 ± 3
20c	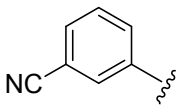	10 ± 1	**20j**	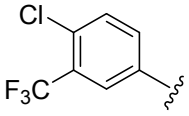	2 ± 1

20d	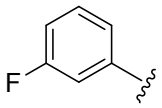	7 ± 1	**20k**	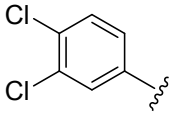	0.12 ± 0.06
20e	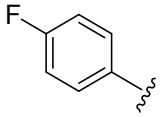	9 ± 1	**20l**	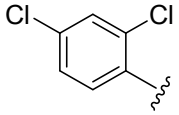	17 ± 2
20f	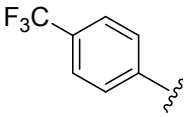	33 ± 7	**20m**	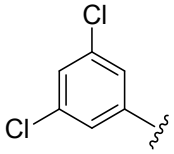	9 ± 2

We then addressed optimization of the oxazole 2-position to adjust the interactions of the important carboxylate moiety (**Table 2**). While the rigidization of the flexible ethyl linker by a double bond resulted in a twofold loss of potency (**22a**), introduction of an additional methylene (**22b**) further improved the inhibitory activity. Replacement of the propyl bridge by a rigid phenyl linker (**22d**) demonstrated that optimal interactions of the carboxylate are achieved at a distance of 4 bonds from the oxazole core. The conformationally restrained *ortho* and *para* substituted benzoic acids did not retain this high potency (**22c** and **22e**).

Table 2. Optimization of the linker in 2-position of the oxazole core.

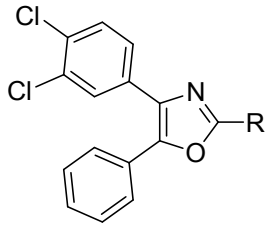

Cpd	R	IC50 [µM]
20k	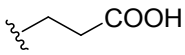	0.12 ± 0.06
22a	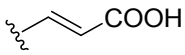	0.51 ± 0.08
22b	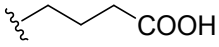	0.058 ± 0.005
22c	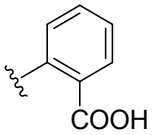	15 ± 1
22d	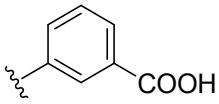	0.15 ± 0.04
22e	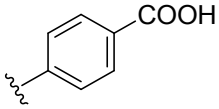	12 ± 2

Finally, the impact of the phenyl substituent in 5-position of the oxazole was investigated, while 3,4-dichlorophenyl substituent in the 4-position and the propionic acid in the 2-position were

maintained (**Table 3**). When the phenyl substituent was omitted, the potency dropped dramatically (**25**) but was partially restored by introduction of a bromine substituent (**26**). Pyridine moieties were not favored (**28a** and **28b**) while almost every substituent in *ortho* or *meta* position was well-tolerated, with a slight preference for fluorine (compound **28e**) or linear substituents such as nitrile (**28g**) or ethinyl (**28j**). However, no further potency improvement over **22b** and **22d** was achieved rendering these oxaprozin derivatives as most active sEH-P inhibitors for further characterization.

Table 3. Optimization of the 5-position of the oxazole core.

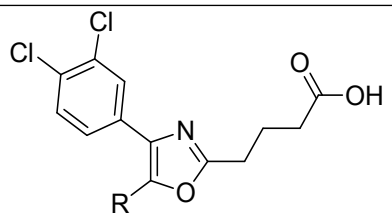

Cpd	R	IC50 [μM]	Cpd	R	IC50 [μM]
25	H	>50	**28e**	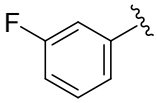	0.12 ± 0.02
26	Br	3 ± 1	**28f**	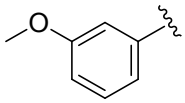	0.31 ± 0.05
22b	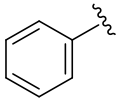	0.058 ± 0.005	**28g**	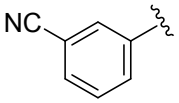	0.12 ± 0.01

28a	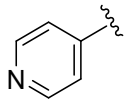	20 ± 1	**28h**	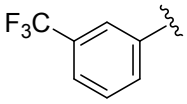	0.41 ± 0.19
28b	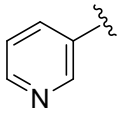	4 ± 1	**28i**	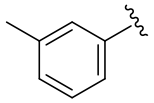	0.31 ± 0.04
28c	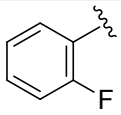	0.31 ± 0.04	**28j**	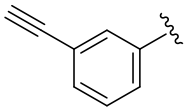	0.14 ± 0.01
28d	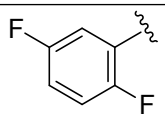	0.28 ± 0.01	**28k**	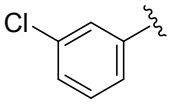	0.23 ± 0.11

In vitro characterization of 22b and 22d

To verify binding of the most potent compound **22b** to sEH-P, orthogonal biophysical assays were performed. Differential scanning fluorimetry (DSF), also known as thermal shift assay, was conducted with the N-terminal domain and the C-terminal domain of sEH. The N-terminal domain was stabilized by **22b**, while the reference inhibitor of the sEH hydrolase activity CIU (*N*-cyclohexyl-*N*'-(4-iodophenyl)urea)[19] had no stabilizing effect on the phosphatase domain (**Figure 2A**). A full list of the DSF experiments with additional reference inhibitors is included in the Supporting Information. In contrast, **22b** did not stabilize the C-terminal domain which melting point was instead significantly increased by CIU (**Figure 2B**). Isothermal titration calorimetry revealed tight binding of **22b** to the N-terminal domain of sEH with a K_d value of 0.3 μM (**Figure**

2C). The analysis of the thermodynamic properties of binding revealed balanced enthalpic and entropic contributions to binding enthalpy (**Figure 2D**).

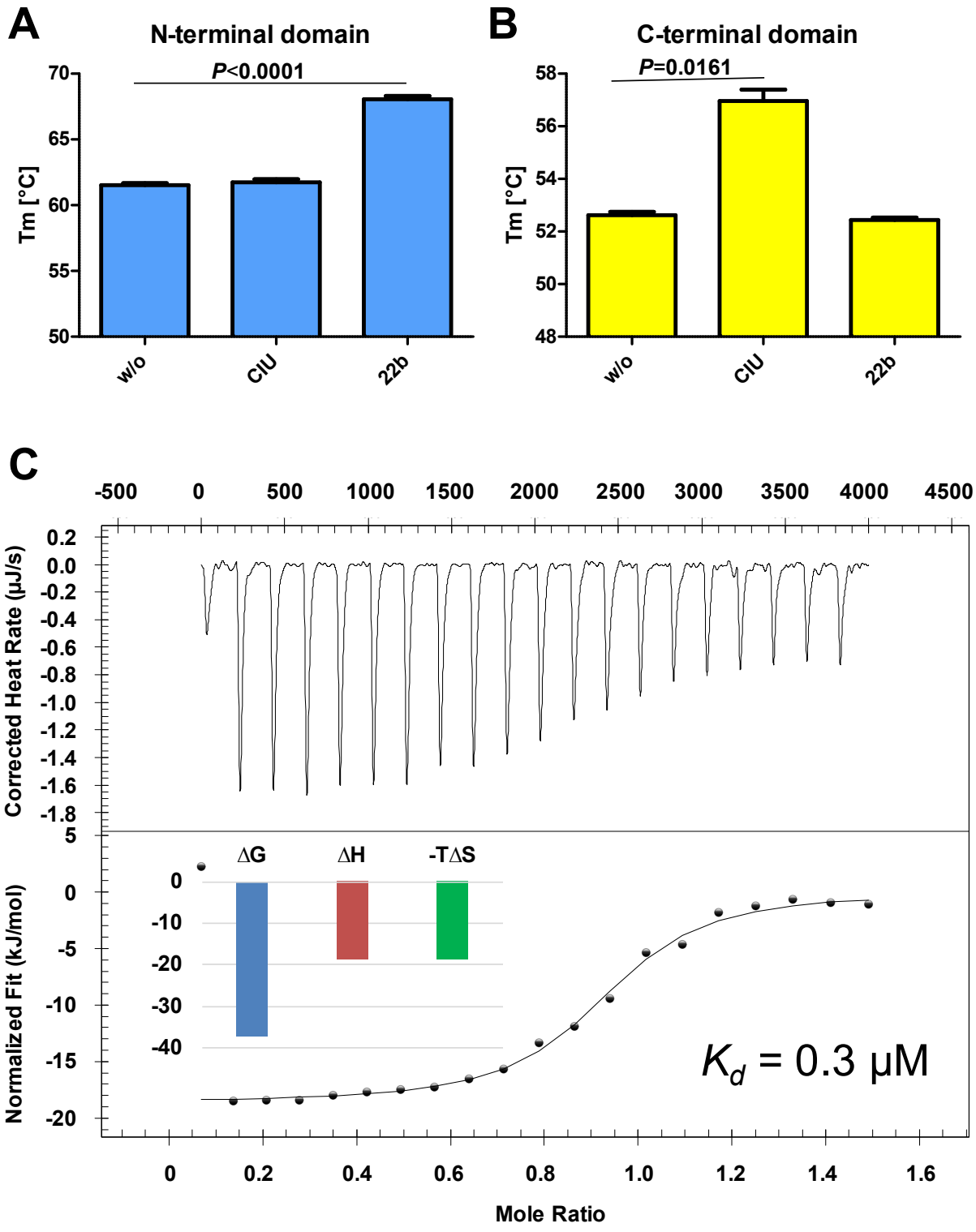
A
N-terminal domain
P<0.0001
Tm [°C]
70
65
60
55
50
w/o
ClU
22b
B
C-terminal domain
P=0.0161
Tm [°C]
58
56
54
52
50
48
w/o
ClU
22b
C
-500
0
500
1000
1500
2000
2500
3000
3500
4000
4500
Corrected Heat Rate (µJ/s)
0.2
0.0
-0.2
-0.4
-0.6
-0.8
-1.0
-1.2
-1.4
-1.6
-1.8
ΔG
ΔH
-TΔS
5
0
-10
-20
-30
-40
Normalized Fit (kJ/mol)
0
-5
-10
-15
-20
K_d = 0.3 µM
0
0.2
0.4
0.6
0.8
1.0
1.2
1.4
1.6
Mole Ratio

Figure 2. **Biophysical characterization of 22b.** A. **22b**, but not sEH hydrolase inhibitor CIU stabilized the N-terminal domain of sEH in differential scanning fluorimetry (DSF) assay. B. **22b** did not stabilize the C-terminal domain of sEH, in contrast to CIU. The concentration of the inhibitors in the DSF experiments was 50 μM. Statistical significance of the measured melting points compared to the DMSO control was determined by a two-tailored T-test using GraphPad Prism (version 7.05; GraphPad Software, Inc.). C. ITC measurement of the complex formation of **22b** and N-terminal sEH domain. Shown are raw binding heats of each injection (top panel) as well as normalized binding heats fitted to a single binding site model (solid line). The thermodynamic parameters of this titration experiment are shown in the insert.

Compound **5** (oxaprozin) is an approved non-selective inhibitor of cyclooxygenases 1 and 2. Therefore, the inhibitory potency of **22b** towards cyclooxygenases was investigated. **22b** exhibited slightly lower potency towards both cyclooxygenase isoforms compared to **5,** which inhibits COX-1 with an IC_{50} of 0.74 μM (29%CV) and COX-2 with an IC_{50} of 0.11 μM (38%CV). Furthermore, agonistic potency towards peroxisome proliferator-activated receptor gamma (PPARγ) and retinoid X receptor alpha (RXRα) was observed, which needs to be considered when using **22b** in cellular assays.

Table 4. Selectivity screen of **22b** and **5** (oxaprozin) towards diverse targets of fatty acid mimetics. All values are measures at least as duplicate ($n \geq 2$). Values for nuclear receptors are mean ± SD% transactivation of reference agonist; inactive - no statistically significant reporter transactivation at the indicated concentration

Target	**Effect**	
	22b	**5**
Cyclooxygenase 1 (COX-1)	IC_{50} = 1.2 μM (20% CV)	IC_{50} = 0.74 μM (29%CV)
Cyclooxygenase 2 (COX-2)	IC_{50} = 0.42 μM (9.6% CV)	IC_{50} = 0.11 μM (38%CV)
PPARα	inactive at 10 μM	inactive at 10 μM
PPARβ/δ	inactive at 10 μM	inactive at 10 μM
PPARγ	29±1% at 10 μM	inactive at 10 μM
FXR	inactive at 10 μM	inactive at 10 μM
LXRα	inactive at 10 μM	inactive at 10 μM
LXRβ	inactive at 10 μM	inactive at 10 μM
RXRα	77±2% at 10 μM	14.4±0.4% at 10 μM

In order to understand the structural basis of sEH-P inhibition by oxazole-based compounds, co-crystallization experiments of sEH-P domain with oxazole inhibitors **22b** and **22d** were performed. While the most affine inhibitor **22b** did not yield crystals, **22d** was co-crystallized with the sEH-P. **Figure 3A** shows the N-terminal domain, with the bound compound **22d**, while **Figure 3B** and **Figure 3C** show details of the inhibitor interaction. The main interaction of **22d** with the protein was mediated by its carboxyl group that formed hydrogen bonds with the residues Asn124 and Asn189 as well as three water molecules. Two of these water molecules were tightly coordinated by a magnesium ion which was present in the active site. In addition, the nitrogen of the oxazole ring formed a water-mediated hydrogen bond with the backbone NH of Val19. The aromatic oxazole system exhibited aromatic edge-to-face interactions with the side chain of Phe41. The phenyl substituents fitted tightly into a deeply buried hydrophobic pockets. **Figure 3C** shows that the phenyl substituent in the 5-position of the oxazole core of the inhibitor is in close proximity to the amino acids Trp126, Phe92, Leu60, Trp63, Leu53, and Phe41 that constitute the most hydrophobic surface area of the binding site. Furthermore, these residues belong to a region in the structure where the most prominent structural changes upon inhibitor binding were observed. The environment around the 3,5-dichloro phenyl group in the 4-position of the oxazole core comprises three hydrophobic amino acids Ile96, Val19 and Trp126 in close proximity to this ring system. Here, the importance of the chlorine substituents can be explained by contacts towards backbone carbonyl oxygens of Phe92 and Ile 96, comparable to ones observed by Heroven et al.[20] and Falke et al.[21] (**Figure 3D**). The phenyl ring in the 2-position of the oxazole core carrying the carboxyl group was positioned in close proximity to the entrance of the active site. The amino acids Phe20, Phe41, Val19 and Thr50 were shielding one side of the phenyl ring while the other side was mainly solvent exposed.

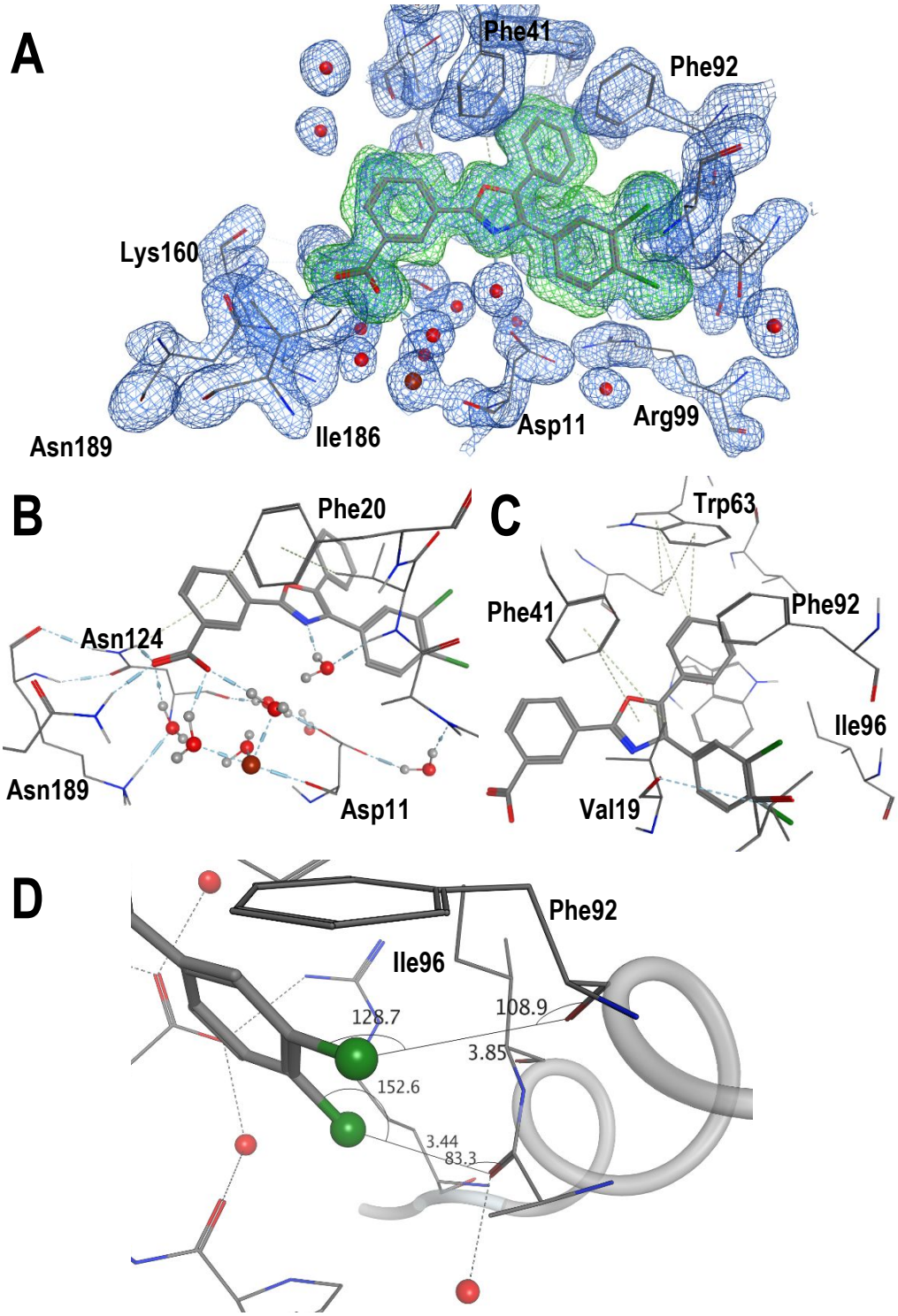
A
Phe41
Phe92
Lys160
Asn189
Ile186
Asp11
Arg99
B
Phe20
Asn124
Asn189
Asp11
C
Trp63
Phe41
Phe92
Ile96
Val19
D
Phe92
Ile96
128.7
108.9
3.85
152.6
3.44
83.3

Figure 3. X-ray structure of **22d** in complex with the N-terminal domain of sEH (PDB code 5MWA)**.** A. $2F_o$-F_c electron density map at 1σ of **22d** in the binding pocket (blue mesh) as well as the polder omit map at 3σ (green mesh). B. The interactions of the carboxylate head group with the Mg^{2+} ion are mediated by water molecules. C. Hydrophobic interaction of the phenyl residues. D. Interactions of the chlorine substituents with backbone carbonyl atoms.

In order to investigate the applicability of **22b** in typical model organisms in vivo, the inhibitory potency against full length (fl) human, mouse, and rat sEH was compared (**Table 5**). **22b** inhibited the phosphatase activity of the human full length enzyme, however, its potency was significantly decreased compared to the isolated N-terminal domain. Furthermore, the sEH-H activity was also affected showing an IC_{50} of about 9 μM. Most strikingly, **22b** did not inhibit neither hydrolase nor phosphatase activity of the mouse sEH, while rat sEH-P was selectively impaired.

Table 5. Inhibitory activity of **5** (oxaprozin) and **22b** against sEH enzymes from different species

	Human fl sEH		Mouse fl sEH		Rat fl sEH	
	sEH-H	sEH-P	sEH-H	sEH-P	sEH-H	sEH-P
5 IC_{50} (μM)	>300	70.0 ± 3.0	>300	35.5 ± 5.8	>300	62.5 ± 1.9
22b IC_{50} (μM)	9.5 ± 0.5	4 ± 1	>30	>30	>30	2.8 ± 2.2

In order to explain the lack of activity against mouse sEH, residues in close proximity to the inhibitor in the enzyme were investigated. Five amino acids which differed between the human and the mouse enzymes were identified including Val19Ile, Phe20Ala, Phe41Tyr, Leu60Phe, Ile96Met. The rat protein features the same sequence changes as mouse protein except Phe41 which remains unchanged in the rat protein compared to human sEH. To investigate the influence of these five sequence changes to inhibitor binding, in silico mutagenesis of the sEH-P complex structure was performed using MOE software suite. **Figure 4** shows the influence of the mutations on the shape of the binding site. We identified Phe41Tyr as the most significant difference between the human and mouse enzymes, while Leu60Phe might also have a slight influence on the inhibitor binding. The reason for the prominent effect of Phe41Tyr mutation on inhibitor binding is the addition of the hydroxyl group which collides with the oxazole core of **22d**, efficiently blocking the inhibitor binding. Phe41 is not altered in rat sEH, which supports the model shown in **Figure 4**.

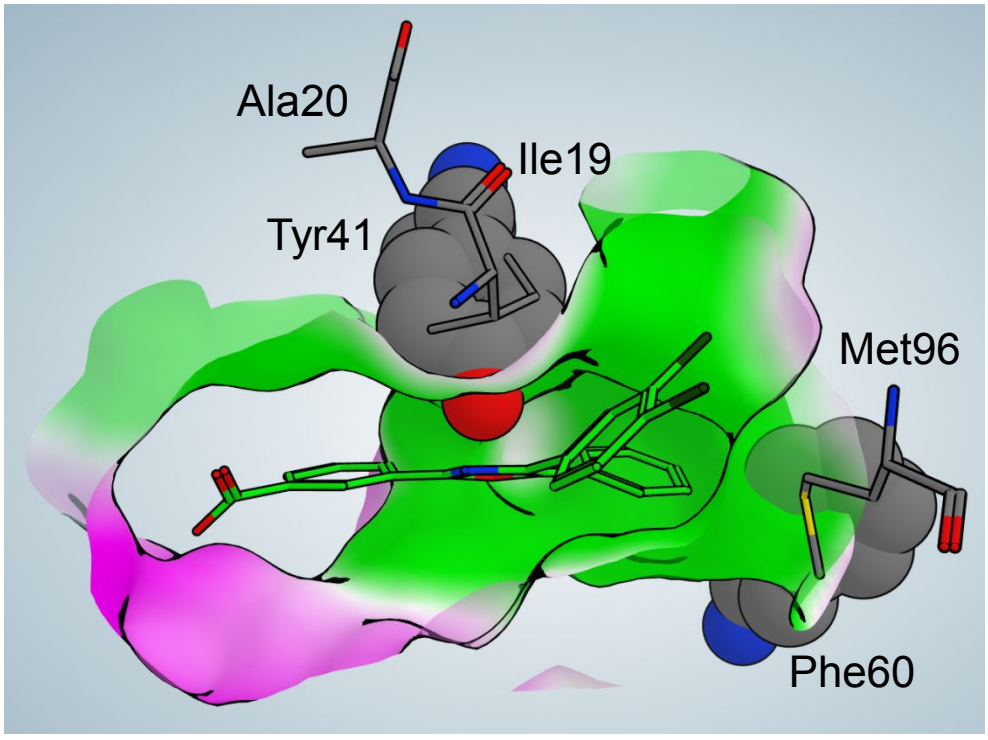

Figure 4. Analysis of sequence changes in different species and its implication in inhibitor potency. The crystal structure of the human sEH-P was used to calculate the surface of the receptor binding site (shown in green for hydrophobic and pink for hydrophilic areas), with the bound inhibitor **22d**. In addition, the 5 amino acids that differ between the human and mouse sEH in the binding pocket were mutated in silico and are shown in the picture, where the two most significant changes Tyr41 and Phe60 are shown as space filling representations.

Structural analysis of **22d** binding to sEH-P suggest possible explanation of the pronounced differences between the inhibition of the full length enzyme and the isolated sEH-P domain. Although the structure was refined at high resolution (1.55 Å), the position of the amino acids 74-84 and 131-138 could not be determined due to disorder resulting in the lack of interpretable electron density in these regions. A comparison of the crystal structure with the crystallized full length protein revealed that the areas that were not modeled in our structure have quite high B-factors in full length sEH (pdb: 5alu)[22]. Additionally, the protein sequences of the human and the mouse enzyme show high sequence variability in the areas 82- 88 and 89 -100 as well as 130-146. Comparison to one of the published full length sEH crystal structures (pdb: 5alu)[22] showed that the binding of the inhibitor led to a prominent induced fit in the binding site (**Figure 5A**). The phenyl ring in the 5-position of the oxazole core pushes Leu60 and Trp126 towards the interface between the N-terminal and the C-terminal domain. This leads to a movement of the interacting residues Asp128 and Arg130. These structural changes lead to shift in the residues Met145, His146, and Glu142, which are in contact with the interface between the N-terminal and the C-terminal domain (**Figure 5B** and **5C**).

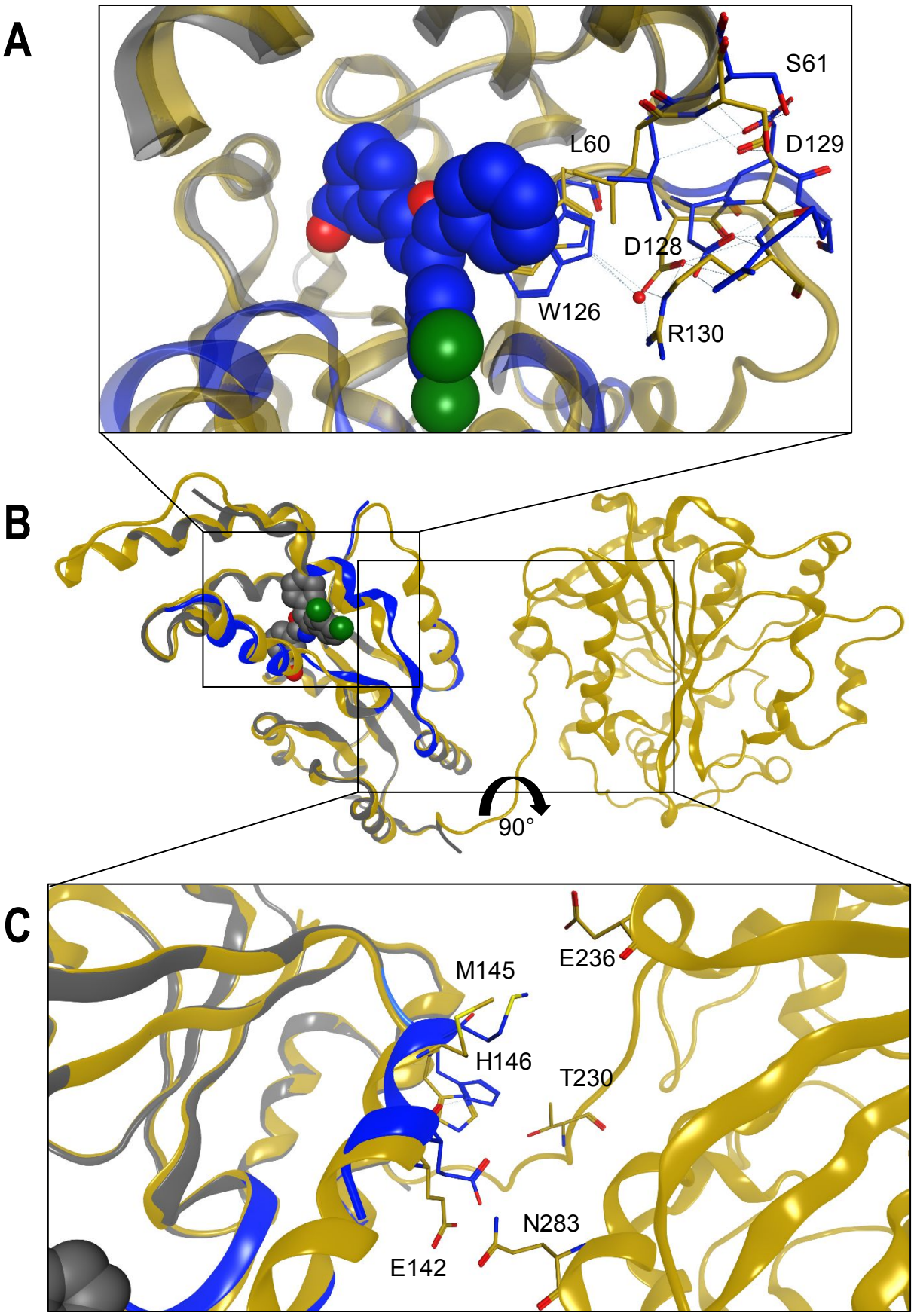
A
S61
L60
D129
D128
W126
R130
B
90°
C
M145
E236
H146
T230
N283
E142

Figure 5. Induced fit binding of **22d** to the N-terminal domain leads to structural distortion of the interface to the C-terminal domain. A. Binding site of 22d; B. global view on the superposed proteins (PDB codes 5mwa and 5alu); C. Interface between the N-terminal and the C-terminal domain.

The structural data suggests that there is a probability that the C-terminal domain hinders the binding of **22d** to the N-terminal domain in the context of the full length enzyme. Therefore, we performed kinetic experiments to validate the mode of inhibition and determine the K_i of **22b** towards the isolated N-terminal domain and the full length sEH (**Figure 6**). We used DiFMUP, an sEH-P substrate with only one phosphate moiety, as a substrate and determined a K_m value of 219.9 μM for the isolated N-terminal domain and a K_m value of 628.5 μM for the full length sEH. We were able to demonstrate that **22b** is a competitive inhibitor under both conditions tested. We determined a K_i value of 0.05 μM for the isolated N-terminal domain and a K_i value of 4.8 μM for the full length sEH, which is in agreement with the discrepancy we observe for the IC_{50} values using FDP as a substrate.

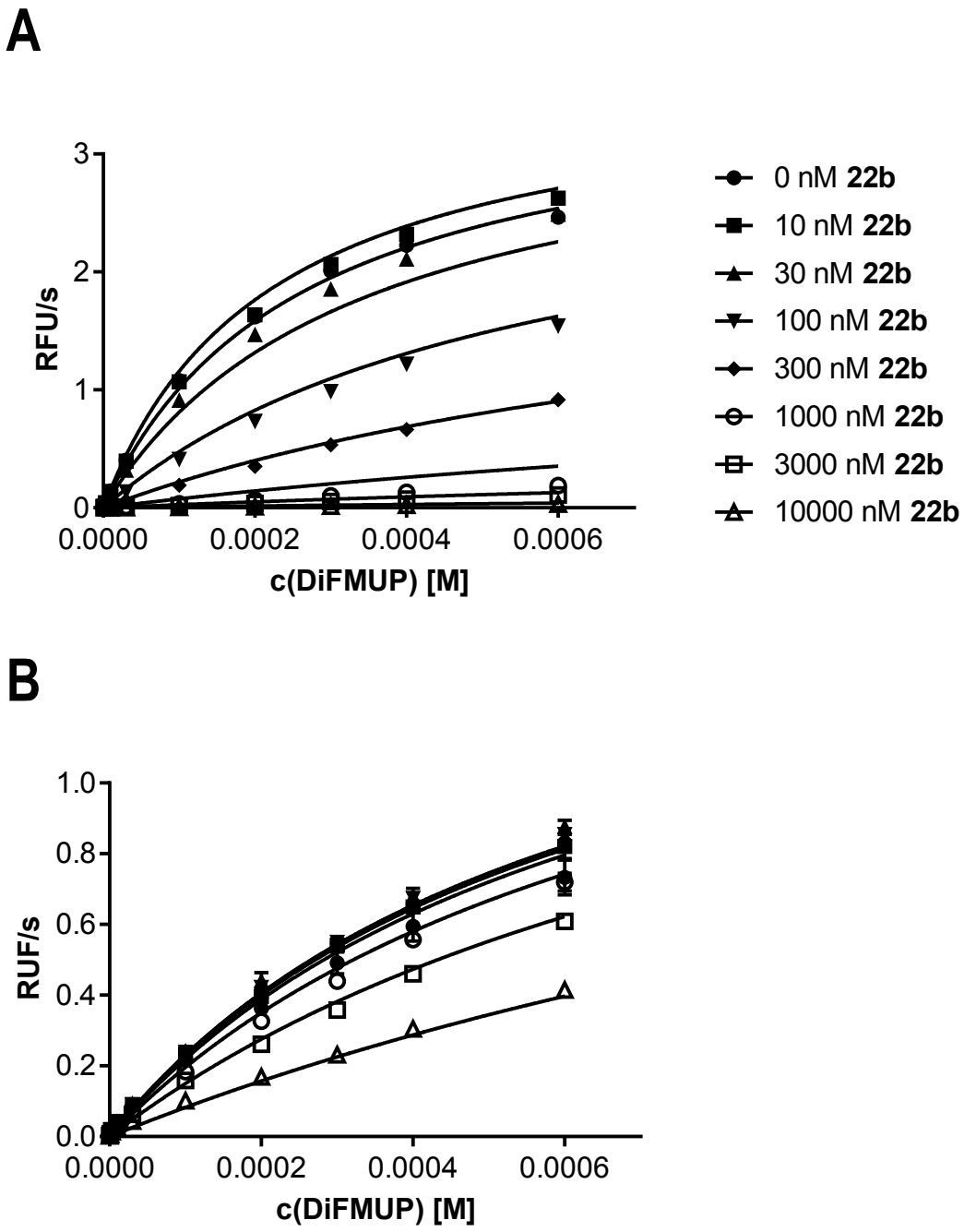

Figure 6. K_i determination of **22b** on the isolated sEH-P domain (A) as well as on the sEH-FL (B) by a mixed model inhibition fit in GraphPad (version 7.05; GraphPad Software, Inc.).

Due to the decreased activity of **22b** against full length sEH-P compared to the isolated N-terminal domain as well as its inhibitory activity against sEH-H in the full length enzyme (**Table 5**), we also evaluated and compared the inhibitory behavior of previously published sEH-P inhibitors. Initial DSF experiments showed that only compounds **2** and **22b** are able to stabilize the N-terminal domain of sEH (**Table 6** and Supporting Information). **1** (SDS) displays inhibitory potency against N-terminal and full length sEH-P, while leaving sEH-H almost unaffected. **2** (*N*-acetyl-*S*-farnesyl-L-cysteine) potently inhibited the phosphatase activity of the single N-terminal domain and the full length sEH without affecting hydrolase activity. In contrast, **4** (ebselen) potently and unselectively inhibited both activities of separated sEH domains and the full length enzyme. **22b** turned out as most potent inhibitor of the phosphatase activity of the N-terminal domain. However, as mentioned above, the activity towards the full length sEH-P was markedly reduced and in the full length protein, both domains were inhibited with similar IC_{50} values (**Table 6**). These results were surprising due to the fact that the initial screening hit **5** (oxaprozin) inhibited the N-terminal domain, while leaving the sEH-H unaffected[16]. Taken together, the weak activity of current inhibitors limits their applications as chemical probes in cellular assay systems and interspecies differences in the sEH-P active site need to be considered in murine model systems. Furthermore, reported posttranslational modifications of sEH by nitration[23] or phosphorylation[12] might also influence inhibitor binding.

Table 6. DSF experiments with the isolated N-terminal sEH domain and inhibitory activity of sEH-P inhibitors against isolated human sEH domains and full length human sEH enzyme.

Compound	sEH-P DSF [°C]	sEH-H IC_{50} [µM]	sEH-P IC_{50} [µM]	fl sEH-H IC_{50} [µM]	fl sEH-P IC_{50} [µM]

1 (SDS)	-0.6 ± 1.8	101 ± 22	2.3 ± 0.2	>300	5.5 ± 0.4
2 (*N*-acetyl-*S*-farnesyl-L-cysteine)	3.4 ± 0.7	>300	0.55 ± 0.01	>300	2.04 ± 0.13
4 (ebselen)	n.d.	0.11 ± 0.01	0.29 ± 0.01	0.30± 0.01	0.42 ± 0.03
22b	6.6 ± 0.8	12 ± 1	0.058 ± 0.005	9.5 ± 0.5	4 ± 1

In order to characterize **22b** as a suitable inhibitor to study the role of sEH-P in vivo, a PK/PD study was conducted. After acute administration of 30 mg/kg p.o. to male SD rats, the evolution of the plasma concentration of **22b** was monitored over 8 hours. **22b** displayed excellent exposure, reaching a maximum concentration of 48 μg/ml (128 μM) and a calculated plasma half-life of 7 hours (**Figure 7A**). Despite of the inhibition of the conversion of the artificial fluorogenic substrate PHOME by sEH-H observed in vitro (**Table 6**), treatment with **22b** did not influence the ratio of the main epoxy fatty acids metabolized by sEH-H to their respective diols, quantified in rat plasma by LC-MS/MS (**Figure 7B**). However, the ratios of different LPAs to their corresponding monoacylglycerols (MAGs) were significantly shifted towards the LPA species as expected (**Figure 7C**). This is a strong indication that the role of sEH-P is determined by the degradation of different LPAs, as suggested in two independent studies by Morisseau[8] and Oguro[9]. In order to confirm that the results we obtained in vivo are transferable to a human system, we incubated human peripheral blood mononuclear cells (PMBCs) with 30 μM of **22b**. In this system we could also observe the reduction of the MAG/LPA ratios (Supporting

Information **Figure S2**). Still, properly chosen control substances are required for use of **22b** in cellular and in vivo experiments due to residual activity on COX enzymes and some nuclear receptors (**Table 4**).

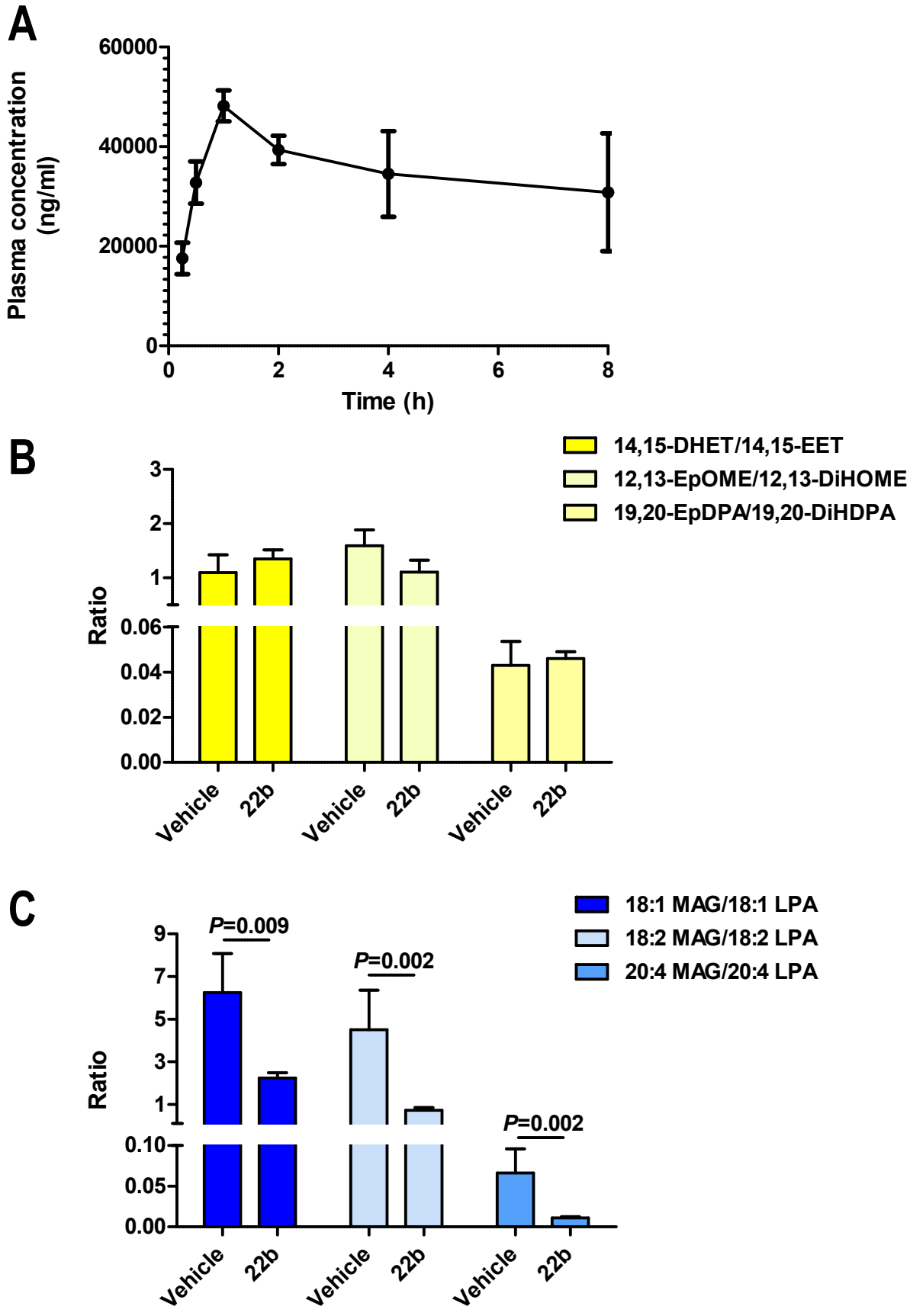
A
Plasma concentration (ng/ml)
60000
40000
20000
0
0
2
4
6
8
Time (h)
B
14,15-DHET/14,15-EET
12,13-EpOME/12,13-DiHOME
19,20-EpDPA/19,20-DiHDPA
Ratio
3
2
1
0.06
0.04
0.02
0.00
Vehicle
22b
Vehicle
22b
Vehicle
22b
C
18:1 MAG/18:1 LPA
18:2 MAG/18:2 LPA
20:4 MAG/20:4 LPA
Ratio
P=0.009
P=0.002
P=0.002
9
7
5
3
1
0.10
0.05
0.00
Vehicle
22b
Vehicle
22b
Vehicle
22b

Figure 7. In vivo studies of 22b in male SD rats. A. Evolution of the plasma concentration of **22b** after acute administration of 30 mg/kg. p.o. in SD rats (n=3) with a peak concentration of C_{max} at 128 μM. B. Ratio of the epoxy fatty acids 14,15-epoxyeicosatrienoic acid (14,15-EET), 12,13-epoxyoctadecenoic acid (12,13-EpOME) and 19,20-epoxydocosapentaenoic acid (19,20-EpDPA) to their respective diols, 14,15-dihydroxyeicosatrienoic acid (14,15-DHET), 12,13-dihydroxy-octadecenoic acid (12,13-DiHOME) and 19,20-dihydroxydocosapentaenoic acid (19,20-EpDPA) quantified in rat plasma 8 hours after acute oral administration of **22b** or vehicle (n=3 per group). C. Ratio of 1-oleyl lysophosphatidic acid (sn1-18:1 LPA), 1-linoleyl LPA (sn1-18:2 LPA), 1-arachidonoyl LPA (sn1-20:4 LPA) and corresponding monoacylglycerol (MAG) species between **22b** and vehicle 8 hours after administration quantified in rat plasma (n=3 per group).

Conclusions

In this study we report the optimization of oxazole-based ligands of the N-terminal domain of sEH. The structure-activity relationships revealed an important role of the 3,4-dichloro phenyl substituent in the 4-position of the oxazole core. Optimization led to the identification of **22b** and **22d** as potent inhibitors of the sEH-P activity in vitro. The reported X-ray structure of a potent ligand **22d** provided first insights into inhibitor binding to N-terminal domain of sEH-P. A prominent induced-fit upon inhibitor binding was observed. Significant interspecies differences in the sEH-P active site which need to be considered using sEH-P inhibitors can be rationalized by the X-ray structure. In vivo studies confirmed **22b** active in rats with favorable pharmacokinetics and revealed involvement of sEH-P in LPA hydrolysis. Hence, this study reports the first in vivo active inhibitor to study the elusive physiological and pathophysiological role of sEH-P.

Experimental Section

Chemistry materials and general procedures

All solvents and chemicals were purchased from Sigma-Aldrich Chemie GmbH (Munich, Germany), Acros Organics (Geel, Belgium), Alfa-Aesar GmbH & Co KG (Karlsruhe, Germany), TCI Europe (Zwijndrecht, Belgium) and Apollo Scientific Ltd. (Manchester, England) and used without further purification. Analytical TLC (thin layer chromatography) was performed with TLC plates F254 from Merck (KGaA, Darmstadt, Germany) visualized with ultraviolet light (254 nm). Column chromatography was performed with technical grade solvent mixtures specified in the corresponding experiment with Fluka silica gel 60 (230−400 mesh ASTM). ^{1}H-NMR spectra were recorded on a Bruker DPX 250 (250 MHz), or AV300 (300 MHz) spectrometer (Bruker, Karlsruhe, Germany). ^{1}H-NMR data are reported in the following order: chemical shift (δ) in ppm downfield relative to tetramethylsilane: internal reference non-deuterated solvent; multiplicity (br, broad; s, singlet; d, doublet; dd, double doublet; t, triplet; q, quadruplet; m, multiplet;); number of protons; approximate coupling constant (*J*) in hertz (Hz). ^{13}C-NMR spectra were recorded on a Bruker AV300 (75 MHz) or AV500 (125 MHz) spectrometer (Bruker, Karlsruhe, Germany). HPLC and mass analyses were performed by a LCMS 2020 from Shimadzu (Duisburg, Germany), under the use of a MultoHigh UC (50 mm × 2 mm) column from CS Chromatography-Service GmbH (Langerwehe, Germany) or a column from Phenomenex Luna 10µ C18(2) 100A (250 x 4.60 mm) for analytical purposes and a Luna 10µ C18(2) (250 x 21.20 mm) column from Phenomenex LTD Deutschland (Aschaffenburg, Germany) for preparative purposes. Condition were as followed: acetonitrile/0.1% aqueous formic acid eluent at 0.5 mL/min (UPLC), 0.1 mL/min (Scout column) or 21 mL/min (semi-preparative) flow rate at room temperature. UV absorption was monitored at 254 and 280 nm, while ESI detector produced positive (+) as well as

negative (-) spectra. Purity of all final compounds was 95% or higher determined by HPLC using following method (except compound **9**): gradient of 50% to 10% acetonitrile within 10 min, 10% acetonitrile were hold for another 10 min. Compound **9** was monitored with an isocratic method with 50 % acetonitrile. Integrated peaks of the chromatogram at (λ = 254 and 280 nm) were used to define purity. MALDI-HRMS was performed on a MALDI LTQ Orbitrap XL instrument (Thermo Scientific, USA).

Methyl 2-((4,5-diphenyloxazol-2-yl)thio)acetate (8). To a solution of 0.75 g 4,5-diphenyloxazole-2-thiol (2.94 mmol, 1.0 equiv) in 10 mL THF was added 0.83 mL triethylamine (5.87 mmol, 2.0 equiv) at room temperature. After 10 min 0.31 mL methyl 2-bromoacetate (3.23 mmol, 1.1 equiv) was added and the mixture stirred overnight following filtration over Celite and concentration of the filtrate under reduced pressure. The residue was purified via column chromatography (eluent: 5/1; Hex / EtOAc) yielding 0.85 g (2.58 mmol, 88%). R_f-Value: 0.28 (8/1; Hex / EtOAc). ^{1}H-NMR (250 MHz, CD_3OD): δ = 7.51 (m, 10H, *Ph*), 4.24 (s, 2H, -C*H*$_2$-), 3.73 (s, 3H, -C*H*$_3$). ESI-MS: *m/z* = 326.0 $[M+H^+]^+$.

2-((4,5-Diphenyloxazol-2-yl)thio)acetic acid (9). In a microwave vial 0.83 g of title compound **8** (2.58 mmol, 1 equiv) was solved in 4 mL of a mixture of MeOH/water/THF (ratio: 1/2/1) adding 0.43 g potassium hydroxide powder (7.65 mmol, 3 equiv). The vial was capped and heated to 70 °C for 15 minutes in the microwave. The solvent was removed, the residue uptaken in 7 mL water, acidified with 10% HCl to pH = 5 and lyophilized. The raw product was recrystallized from EtOAc yielding 0.52 g (1.67 mmol, 65%). R_f-Value (RP): 0.64 (3/1; MeOH/ water). ^{1}H-NMR (250 MHz, $CDCl_3$): δ = 7.46 (m, 10H, *Ph*), 3.94 (s, 2H, -C*H*$_2$-). ^{13}C-NMR (75 MHz, $CDCl_3$):

171.3, 158.1, 146.4, 135.0, 130.5, 127.7, 127.6, 127.4, 127.2, 126.8, 125.3, 35.5. HRMS: calculated: *m/z* = 312.06889; found: *m/z* = 312.06931.

General procedure for the synthesis of oxaprozin derivatives 12, 20a-m and 22a-e. Succinic acid **19**, succinic amide **10**, or corresponding dicarboxylic acid **21a-e** (3 equiv) was dissolved in acetonitrile and treated with triethylamine (3 equiv). After 15 minutes the α-bromoketone (1 equiv), solved in a minimal amount of acetonitrile, was added. The mixture was stirred at 45 °C for 6 hours. The solvent was removed, the residue diluted with ethyl acetate and washed with water and brine. A white resin was isolated. The residue was taken up in acetic acid (10 mL), ammonium acetate (10 equiv) was added and the mixture was heated to reflux for another 3 hours. The mixture was thrown on ice, extracted with ethyl acetate and the residue purified via column chromatography (eluent: 3/1 Hex; / EtOAc +3%AcOH). Yields calculated are based upon the two step reaction starting from the deoxybenzoin. The product was further purified by preparative HPLC yielding white solids.

3-(4,5-Diphenyloxazol-2-yl)propanamide (12). Instead of succinic acid succinic amide was used starting from α-bromo-deoxybenzoin. Yield: 296 mg (68%). R_f -Value: 0.22 (98/2; DCM / MeOH). ^{1}H-NMR (300 MHz, DMSO-d_6): δ = 7.57-7.32 (m, 11H, *Ph*, 1x -N*H*$_2$), 6.87 (br, 1H, 1x -N*H*$_2$), 3.04 (t, 2H, J = 7.3 Hz, C*H*$_2$-CONH$_2$), 2.62 (t, 2H, J = 7.3 Hz, C*H*$_2$-CH$_2$). ^{13}C-NMR (75 MHz, DMSO-*d*$_6$): δ = 172.4, 162.73, 144.4, 134.2, 132.0, 128.8, 128.7, 128.5, 128.4, 128.0, 127.3, 126.2, 31.3, 23.1. HRMS: calculated: *m/z* = 293.12845; found: *m/z* = 293.12880.

General procedure for the synthesis of cyanohydrins compounds 15a-m. To the appropriate benzaldehyde derivative **13a-m** (1 equiv) was added trimethylsilyl cyanide **14** (TMSCN; 1 equiv) followed by triethylamine (0.2 equiv). Only if starting material did not dissolve within 10

minutes, 1 mL DCM was added. The solution was stirred over night at room temperature. The mixture was diluted with DCM, washed with conc. ammonium chloride solution and brine. The organic layer was filtered over silica gel and rinsed with 100 mL DCM. The solvent was removed under reduced pressure and used without further purification. In most cases a liquid was isolated.

2-(2-Fluorophenyl)-2-((trimethylsilyl)oxy)acetonitrile (15a). Yield: 1.28 g (colorless liquid; 96%). R_f -Value: 0.76 (5/1; Hex / EtOAc). ^{1}H-NMR (250 MHz, $CDCl_3$): δ = 7.64 (td, 1H, J = 7.6 Hz, 1.6 Hz, *Ph*-4*H*), 7.45-7.35 (m, 1H, *Ph*-6*H*), 7.23 (td, 1H, J = 7.6 Hz, 1.1 Hz, *Ph*-2*H*), 7.61 (td, 1H, J = 8.7 Hz, 1.1 Hz, *Ph*-5*H*), 5.76 (s, 1H, -CH-), 0.24 (s, 9H, 3x -CH_3). ESI-MS: *m/z* = 195.8 $[M\text{-}CN^-]^-$.

2-(4-Chlorophenyl)-2-((trimethylsilyl)oxy)acetonitrile (15b). Yield: 607 mg (colorless liquid; quant.). R_f -Value: 0.78 (9/1; Hex / EtOAc). ^{1}H-NMR (250 MHz, $CDCl_3$): δ = 7.74-7.70 (m, 1H, *Ph*-5*H*), 7.42-7.32 (m, 3H, *Ph*-3*H*,4*H*,6*H*), 5.80 (s, 1H, -C*H*-), 0.26 (s, 9H, 3x -CH_3). ESI-MS: *m/z* = 211.75 $[M\text{-}CN^-]^-$.

3-(Cyano((trimethylsilyl)oxy)methyl)benzonitrile (15c). Yield: 1.30 g (pale yellow liquid; 94%). R_f -Value: 0.09 (9/1; Hex / EtOAc). ^{1}H-NMR (250 MHz, $CDCl_3$): δ = 7.78 (s, 1H, *Ph*-2*H*), 7.70-7.68 (m, 2H, *Ph*-4*H*,5*H*), 7.56 (d, 1H, J = 7.7 Hz, *Ph*-6*H*), 5.52 (s, 1H, -C*H*-), 0.28 (s, 9H, 3x -CH_3). ESI-MS: *m/z* = 202.9 $[M\text{-}CN^-]^-$.

2-(3-Fluorophenyl)-2-((trimethylsilyl)oxy)acetonitrile (15d). Yield: 1.35 g (pale yellow liquid; quant.). R_f -Value: 0.71 (5/1; Hex / EtOAc). ^{1}H-NMR (250 MHz, $CDCl_3$): δ = 7.43-7.34 (m, 1H, *Ph*-5*H*), 7.26-7.18 (m, 2H, *Ph*-2*H*,4*H*), 7.09 (td, 1H, J = 8.5 Hz, 2.5 Hz, *Ph*-6*H*), 5.49 (s, 1H, -C*H*-), 0.25 (s, 9H, 3x -CH_3). ESI-MS: *m/z* = 195.8 $[M\text{-}CN^-]^-$.

2-(4-Fluorophenyl)-2-((trimethylsilyl)oxy)acetonitrile (15e). Yield: 1.41 g (colorless liquid; quant.). R_f -Value: 0.56 (9/1; Hex / EtOAc). ^{1}H-NMR (250 MHz, $CDCl_3$): δ = 7.49-7.41 (m, 2H, *Ph*-2*H*,6*H*), 7.10 (pt, 2H, J = 8.6 Hz, *Ph*-3*H*,5*H*), 5.47 (s, 1H, -C*H*-), 0.24 (s, 9H, 3x -CH_3). ESI-MS: *m/z* = 195.8 $[M\text{-}CN^-]^-$.

2-(4-(Trifluoromethyl)phenyl)-2-((trimethylsilyl)oxy)acetonitrile (15f). Yield: 601 mg (pale yellow liquid; 88%). R_f -Value: 0.80 (3/1; Hex / EtOAc). ^{1}H-NMR (250 MHz, $CDCl_3$): δ = 7.69 (d, 2H, J = 8.6 Hz, *Ph*-3*H*,5*H*), 7.61 (d, 2H, J = 8.6 Hz, *Ph*-2*H*,6*H*), 5.55 (s, 1H, -C*H*-), 0.27 (s, 9H, 3x -CH_3). ESI-MS: *m/z* = 245.8 $[M\text{-}CN^-]^-$.

4-(Cyano((trimethylsilyl)oxy)methyl)benzonitrile (15g). Yield: 517 mg (yellow liquid; 90%). R_f -Value: 0.57 (9/1; Hex / EtOAc). ^{1}H-NMR (250 MHz, $CDCl_3$): δ = 7.73 (d, 2H, J = 8.5 Hz, *Ph*-3*H*,5*H*), 7.60 (d, 2H, J = 8.6 Hz, *Ph*-2*H*,6*H*), 5.54 (s, 1H, -C*H*-), 0.27 (s, 9H, 3x -CH_3). ESI-MS: *m/z* = 202.0 $[M\text{-}CN^-]^-$.

2-(4-Chlorophenyl)-2-((trimethylsilyl)oxy)acetonitrile (15h). Yield: 2.24 g (yellow liquid; 93%). R_f -Value: 0.88 (9/1; Hex / EtOAc). ^{1}H-NMR (250 MHz, $CDCl_3$): δ = 7.04 (ps, 4H, *Ph*), 5.46 (s, 1H, -C*H*-), 0.24 (s, 9H, 3x -CH_3). ESI-MS: *m/z* = 211.8 $[M\text{-}CN^-]^-$.

2-(4-Methoxyphenyl)-2-((trimethylsilyl)oxy)acetonitrile (15i). Yield: 604 mg (colorless liquid; quant.). R_f -Value: 0.57 (5/1; Hex / EtOAc). ^{1}H-NMR (250 MHz, $CDCl_3$): δ = 7.38 (d, 2H, J = 8.8 Hz, *Ph*-2*H*,6*H*), 6.92 (d, 2H, J = 8.8 Hz, *Ph*-3*H*,5*H*), 5.43 (s, 1H, -C*H*-), 3.82 (s, 3H, O-CH_3), 0.21 (s, 9H, 3x -CH_3). ESI-MS: *m/z* = 209.3 $[M\text{-}CN^-]^-$.

2-(4-Chloro-3-(trifluoromethyl)phenyl)-2-((trimethylsilyl)oxy)acetonitrile (15j). Yield: 722 mg (yellow liquid; 89%). R_f -Value: 0.87 (5/1; Hex / EtOAc). ^{1}H-NMR (250 MHz, $CDCl_3$): δ = 7.79 (s, 1H, *Ph*-2*H*), 7.59 (ps, 2H, *Ph*-5*H*,6*H*), 5.51 (s, 1H, -C*H*-), 0.27 (s, 9H, 3x -CH_3). ESI-MS: *m/z* = 279.7 $[M\text{-}CN^-]^-$.

2-(3,4-Dichlorophenyl)-2-((trimethylsilyl)oxy)acetonitrile (15k). Yield: 673 mg (orange liquid; 98%). R_f -Value: 0.69 (3/1; Hex / EtOAc). ^{1}H-NMR (250 MHz, $CDCl_3$): δ = 7.57 (sd, 1H, J = 2.0 Hz, *Ph*-2*H*), 7.50 (d, 1H, J = 8.3 Hz, *Ph*-5*H*), 7.30 (dd, 1H, J = 8.3 Hz, 2.1 Hz, *Ph*-6*H*), 5.44 (s, 1H, -C*H*-), 0.26 (s, 9H, 3x -CH_3). ESI-MS: *m/z* = 245.7 [M-CN$^-$]$^-$.

2-(2,4-Dichlorophenyl)-2-((trimethylsilyl)oxy)acetonitrile (15l). Yield: 680 mg (yellow liquid; 99%). R_f -Value: 0.82 (5/1; Hex / EtOAc). ^{1}H-NMR (250 MHz, $CDCl_3$): δ = 7.65 (d, 1H, J = 8.4 Hz, *Ph*-6*H*), 7.42 (sd, 1H, J = 2.0 Hz, *Ph*-3*H*), 7.35 (dd, 1H, J = 8.4 Hz, 2.0 Hz, *Ph*-5*H*), 5.73 (s, 1H, -C*H*-), 0.26 (s, 9H, 3x -CH_3). ESI-MS: *m/z* = 248.1 [M-CN$^-$]$^-$.

2-(3,5-dichlorophenyl)-2-((trimethylsilyl)oxy)acetonitrile (15m). Yield: 600 mg (brown liquid; 88%). R_f -Value: 0.88 (5/1; Hex / EtOAc). ^{1}H-NMR (250 MHz, $CDCl_3$): δ = 7.39-7.35 (m, 3H, *Ph*), 5.43 (s, 1H, -C*H*-), 0.27 (s, 9H, 3x -CH_3). ESI-MS: *m/z* = 245.7 [M-CN$^-$]$^-$.

General procedure for the synthesis of deoxybenzoins compounds 17a-m. The appropriate cyanohydrin (2 mmol; 1 equiv) was dissolved in 3 mL abs. THF and cooled to -78°C. LDA (2.1 mmol; 1.05 equiv) was added and left to stir for 30 minutes followed by addition of benzyl bromide **16** (2.2 mmol; 1.1 equiv) in 1 mL THF. The mixture was stirred for 2 hours and then allowed to warm up to RT and stirred overnight. To the mixture was added 1 M TBAF-solution (2 mL, 1 equiv) and stirred for another half an hour. The mixture was diluted with ethyl acetate, washed with saturated. ammonium chloride solution and 0.5 M NaOH solution, dried and the solvent removed. The yellow-orange residue (ca. 600 mg) was purified by column chromatography (eluent: 9/1; Hex / EtOAc). The purified product solidified upon standing.

1-(2-Fluorophenyl)-2-phenylethan-1-one (17a). Yield: 247 mg (yellow oil; 58%). R_f -Value: 0.70 (5/1; Hex / EtOAc). ^{1}H-NMR (250 MHz, DMSO-d_6): δ = 7.86 (td, 1H, J = 7.6 Hz, 1.7 Hz,

Ph-F-4*H*), 7.70-7.61 (m, 1H, *Ph*-F-6*H*), 7.38-7.15 (m, 7H, *Ph*, *Ph*-F-3*H*,5*H*), 4.31 (s, 2H, -CH_2-). ESI-MS: *m/z* = 214.8 $[M+H^+]^+$.

1-(2-Chlorophenyl)-2-phenylethan-1-one (17b). Yield: 202 mg (pale yellow liquid; 44%). R_f -Value: 0.68 (9/1; Hex / EtOAc). ^{1}H-NMR (250 MHz, DMSO-d_6): δ = 7.72 (dd, 1H, J = 7.8 Hz, 1.6 Hz, *Ph*-Cl-6*H*), 7.53-7.48 (m, 2H, Ph-Cl-3*H*,4*H*), 7.72 (td, 1H, J = 6.7 Hz, 1.9 Hz, *Ph*-Cl-5*H*), 7.33-7.29 (m, 2H, *Ph*-3*H*,5*H*), 7.25-7.21 (m, 3H, *Ph*-2*H*,4*H*,6*H*), 4.29 (s ,2H, -CH_2-). ESI-MS: *m/z* = 230.8 $[M]^+$.

3-(2-Phenylacetyl)benzonitrile (17c). Yield: 320 mg (tan solid; 72%). R_f -Value: 0.14 (9/1; Hex / EtOAc). ^{1}H-NMR (250 MHz, DMSO-d_6): δ = 8.49 (s, 1H, *Ph*-CN-2*H*), 8.30 (d, 1H, J = 8.0 Hz, *Ph*-CN-4*H*), 8.11 (d, 1H, J = 7.8 Hz, *Ph*-CN-6*H*), 7.52 (t, 1H, J = 7.8 Hz, *Ph*-CN-5*H*), 7.37-7.23 (m, 5H, *Ph*), 4.46 (s, 2H, -CH_2-). ESI-MS: *m/z* = 219.9 $[M-H^+]^-$.

1-(3-Fluorophenyl)-2-phenylethan-1-one (17d). Yield: 200 mg (yellow solid; 47%). R_f -Value: 0.60 (5/1; Hex / EtOAc). ^{1}H-NMR (250 MHz, DMSO-d_6): δ = 7.90 (d, 1H, J = 7.7 Hz, *Ph*-F-6*H*), 7.81 (dd, 1H, J = 7.7 Hz, 1.5 Hz, *Ph*-F-4*H*), 7.62-7.56 (m, 1H, *Ph*-F-2*H*), 7.49 (td, 1H, J = 9.2 Hz, 2.5 Hz, *Ph*-F-5*H*), 7.35-7.29 (m, 3H, *Ph*-2*H*,4*H*,6*H*), 7.27-7.23 (m, 2H, *Ph*-3*H*,5*H*), 4.41 (s, 2H, -CH_2-). ESI-MS: *m/z* = 214.9 $[M+H^+]^+$.

1-(4-Fluorophenyl)-2-phenylethan-1-one (17e). Yield: 399 mg (pale yellow solid; 93%). R_f -Value: 0.43 (9/1; Hex / EtOAc). ^{1}H-NMR (250 MHz, DMSO-d_6): δ = 8.13 (t, 2H, J = 8.6 Hz, *Ph*-F-3*H*,5*H*), 7.39-7.22 (m, 7H, *Ph*, *Ph*-F-2*H*,6*H*), 4.38 (s, 2H, -CH_2-). ESI-MS: *m/z* = 214.8 $[M+H]^+$.

2-Phenyl-1-(4-(trifluoromethyl)phenyl)ethan-1-one (17f). Yield: 236 mg (white solid; 45%). R_f -Value: 0.70 (3/1; Hex / EtOAc). ^{1}H-NMR (250 MHz, DMSO-d_6): δ = 8.22 (d, 2H, J = 8.0 Hz,

Ph-CF_3-2*H*,6*H*), 7.90 (d, 2H, J = 8.1 Hz, *Ph*-CF_3-3*H*,5*H*), 7.35-7.22 (m, 5H, *Ph*), 4.47 (s, 2H, -CH_2-). ESI-MS: *m/z* = 264.8 $[M+H^+]^+$.

4-(2-Phenylacetyl)benzonitrile (17g). Yield: 213 mg (white solid; 45%). R_f -Value: 0.39 (5/1; Hex / EtOAc). ^{1}H-NMR (250 MHz, DMSO-d_6): δ = 8.20 (d, 2H, J = 8.6 Hz, *Ph*-CN-2*H*,6*H*), 8.03 (d, 2H, J = 8.6 Hz, *Ph*-CN-3*H*,5*H*), 7.38-7.23 (m, 5H, *Ph*), 4.47 (s, 2H, -CH_2-). ESI-MS: *m/z* = 219.9 $[M-H^+]^-$.

1-(4-Chlorophenyl)-2-phenylethan-1-one (17h). Yield: 192 mg (pale yellow oil; 55%). R_f -Value: 0.75 (9/1; Hex / EtOAc). ^{1}H-NMR (250 MHz, DMSO-d_6): δ = 7.93 (d, 2H, J = 8.6 Hz, *Ph*-Cl-2*H*,6*H*), 7.42 (d, 2H, J = 8.6 Hz, *Ph*-Cl-3*H*,5*H*), 7.35-7.23 (m, 5H, *Ph*), 4.25 (s, 2H, -CH_2-). ESI-MS: *m/z* = 230.8 $[M+H^+]^+$.

1-(4-Methoxyphenyl)-2-phenylethan-1-one (17i). Yield: 286 mg (yellow liquid; 63%). R_f -Value: 0.36 (5/1; Hex / EtOAc). ^{1}H-NMR (250 MHz, $CDCl_3$): δ = 7.99 (d, 2H, J = 8.5 Hz, *Ph*-OCH_3-2*H*,6*H*), 7.30-7.20 (m, 5H, *Ph*), 6.92 (d, 2H, J = 8.5 Hz, *Ph*-OCH_3-3*H*,5*H*), 4.23 (s, 2H, -CH_2-), 3.85 (s, 3H, -CH_3). ESI-MS: *m/z* = 226.9 $[M+H]^+$.

1-(4-Chloro-3-(trifluoromethyl)phenyl)-2-phenylethan-1-one (17j). Yield: 213 mg (colorless liquid; 45%). R_f -Value: 0.53 (5/1; Hex / EtOAc). ^{1}H-NMR (250 MHz, DMSO-d_6): δ = 8.32 (pd, 2H, *Ph*-3CF_3,4Cl-2*H*,6*H*), 7.92 (d, 1H, J = 8.8 Hz, *Ph*-3CF_3,4Cl -5*H*), 7.36-7.21 (m, 5H, *Ph*), 4.49 (s, 2H, -CH_2-). ESI-MS: *m/z* = 299.7 $[M+H^+]^+$.

1-(3,4-Dichlorophenyl)-2-phenylethan-1-one (17k). Yield: 258 mg (pale yellow solid; 49%). R_f -Value: 0.59 (3/1; Hex / EtOAc). ^{1}H-NMR (250 MHz, DMSO-d_6): δ = 8.23 (sd, 1H, J = 2.0 Hz, *Ph*-3,4Cl-2*H*), 7.99 (dd, 1H, J = 8.3 Hz, 2.1 Hz, *Ph*-3,4Cl-6*H*), 7.81 (d, 1H, J = 8.3 Hz, *Ph*-3,4Cl-5*H*),7.34-7.21 (m, 5H, *Ph*), 4.42 (s, 2H, -CH_2-). ESI-MS: *m/z* = 265.9 $[M+H^+]^+$.

1-(2,4-Dichlorophenyl)-2-phenylethan-1-one (17l). Yield: 167 mg (pale yellow liquid; 31%). R_f -Value: 0.65 (9/1; Hex / EtOAc). ^{1}H-NMR (250 MHz, $CDCl_3$): δ = 7.73 (sd, 1H, J = 2.0 Hz, *Ph*-2,4-diCl-3*H*), 7.35-7.19 (m, 7H, *Ph*, *Ph*-2,4-diCl-5*H*,6*H*), 4.24 (s, 2H, -CH_2-). ESI-MS: *m/z* = 265.8 $[M+H^+]^+$.

1-(3,5-Dichlorophenyl)-2-phenylethan-1-one (17m). Yield: 151 mg (pale yellow liquid; 26%). R_f -Value: 0.60 (9/1; Hex / EtOAc). ^{1}H-NMR (250 MHz, DMSO-d_6): δ = 8.01 (sd, 2H, J = 1.9 Hz, *Ph*-3,5-diCl-2*H*,6*H*), 7.92 (sd, 1H, J = 1.9 Hz, *Ph*-3,5-diCl-4*H*), 7.36-7.23 (m, 5H, *Ph*), 4.44 (s, 2H, -CH_2-). ESI-MS: *m/z* = 265.9 $[M+H^+]^+$.

General procedure for the synthesis of α-bromoketones compounds 18a-m. In chloroform was solved the deoxybenzoin derivative (1 equiv) and bromine (1 equiv), solved in chloroform as well, was slowly added and heated to reflux for 2 hours. The mixture was diluted with dichloromethane and washed with water and brine, dried and concentrated under reduced pressure. The resulting liquid was used immediately without further purification.

3-(4-(2-Fluorophenyl)-5-phenyloxazol-2-yl)propanoic acid (20a). Yield: 58 mg (34%). R_f -Value: 0.39 (3/1; Hex / EtOAc +3% AcOH). ^{1}H-NMR (300 MHz, DMSO-d_6): δ = 12.31 (s, 1H, -COO*H*), 7.60-7.46 (m, 2H, *Ph*-F-4*H*,6*H*), 7.59-7.39 (m, 7H, *Ph*, *Ph*-F-3*H*,5*H*), 3.09 (t, 2H, J = 7.0 Hz, -CH_2-COOH), 2.79 (t, 2H, J = 7.0 Hz, -CH_2-CH_2). ^{13}C-NMR (75 MHz, DMSO-d_6): δ = 173.0, 162.4, 131.3, 131.3, 130.8, 130.7, 128.7, 128.4, 127.9, 124.8, 124.8, 124.7, 116.1, 115.8, 30.1, 22.8. HRMS: calculated: *m/z* = 312.10305; found: *m/z* = 312.10411.

3-(4-(2-Chlorophenyl)-5-phenyloxazol-2-yl)propanoic acid (20b). Yield: 82 mg (29%; hygroscopic). R_f -Value: 0.49 (3/1; Hex / EtOAc +3% AcOH) ^{1}H-NMR (300 MHz, DMSO-d_6): δ = 12.33 (s, 1H, -COO*H*), 7.69-7.28 (m, 9H, *Ph*-Cl, *Ph*), 3.06 (t, 2H, J = 7.0 Hz, CH_2-COOH), 2.78 (t, 2H, J = 7.0 Hz, -CH_2-CH_2).^{13}C-NMR (75 MHz, DMSO-d_6): δ = 173.0, 163.0, 141.8, 135.7,

133.3, 132.4, 131.8, 131.1, 130.1, 128.5, 128.0, 127.8, 127.8, 125.8, 30.2, 22.9. HRMS: calculated: *m/z* = 328.07350; found: *m/z* = 328.07482.

3-(4-(3-Cyanophenyl)-5-phenyloxazol-2-yl)propanoic acid (20c). Yield: 39 mg (18%). R_f -Value: 0.76 (3/1; Hex / EtOAc +3% AcOH). ^{1}H-NMR (300 MHz, DMSO-d_6): δ = 12.36 (s, 1H, -COO*H*), 7.93 (s, 1H, *Ph*-CN-2*H*), 7.85 (d, 1H, J = 7.9 Hz, *Ph*-CN-4*H*), 7.81 (d, 1H, J = 7.9 Hz, *Ph*-CN-6*H*), 7.61 (t, 1H, J = 7.8 Hz, *Ph*-CN-5*H*), 7.55-7.51 (m, 3H, *Ph*-2*H*,4*H*,6*H*), 7.49-7.40 (m, 2H, *Ph*-3*H*,5*H*), 3.07 (t, 2H, J = 7.0 Hz, -CH_2-COOH), 2.79 (t, 2H, J = 7.0 Hz, -CH_2-CH_2).^{13}C-NMR (75 MHz, DMSO-d_6): δ = 173.0, 162.8, 145.7, 133.2, 132.3, 131.7, 130.4, 130.0, 129.3, 129.1, 128.8, 127.8, 127.5, 126.6, 118.4, 111.8, 30.1, 22.8. HRMS: calculated: *m/z* = 319.10772; found: *m/z* = 319.10865.

3-(4-(3-Fluorophenyl)-5-phenyloxazol-2-yl)propanoic acid (20d). Yield: 57 mg (24%). R_f -Value: 0.23 (3/1; Hex / EtOAc +3% AcOH). ^{1}H-NMR (300 MHz, DMSO-d_6): δ = 12.33 (s, 1H, -COO*H*), 7.55-7.53 (m, 2H, *Ph*-3*H*,5*H*), 7.48-7.41 (m, 4H, *Ph*-2*H*,4*H*,6*H*, *Ph*-F-2*H*), 7.39 (d, 1H, J = 7.8 Hz, *Ph*-F-6*H*), 7.31 (dd, 1H, J = 9.4 Hz, 1.1 Hz, *Ph*-F-4*H*), 7.18 (td, 1H, J = 7.8 Hz, 1.1 Hz, *Ph*-F-5*H*), 3.06 (t, 2H, J = 6.9 Hz, -CH_2-COOH), 2.78 (t, 2H, J = 7.0 Hz, -CH_2-CH_2). ^{13}C-NMR (75 MHz, DMSO-d_6): δ = 173.0, 162.5, 145.2, 134.3, 132.9, 130.7, 128.9, 128.0, 126.6, 123.1, 115.0, 113.8, 30.2, 22.8. HRMS: calculated: *m/z* = 312.10305; found: *m/z* = 312.10417.

3-(4-(4-Fluorophenyl)-5-phenyloxazol-2-yl)propanoic acid (20e). Yield: 53 mg (19%). R_f -Value: 0.30 (3/1; Hex / EtOAc +3% AcOH). ^{1}H-NMR (300 MHz, DMSO-d_6): δ = 12.31 (s, 1H, -COO*H*), 7.60-7.56 (m, 2H, *Ph*-F-2*H*,6*H*), 7.53-7.50 (m, 2H, *Ph*-F-3*H*,5*H*), 7.47-7.39 (m, 3H, *Ph*-2*H*,4*H*,6*H*), 7.49 (t, 2H, J = 8.9 Hz, *Ph*-3*H*,5*H*), 3.06 (t, 2H, J = 7.1 Hz, -CH_2-COOH), 2.78 (t, 2H, J = 7.1 Hz, -CH_2-CH_2).^{13}C-NMR (75 MHz, DMSO-d_6): δ = 173.0, 163.3, 162.3, 160.1, 144.4,

133.3, 129.4, 129.3, 128.9, 128.8, 128.4, 128.3, 128.2, 126.2, 115.7, 115.4, 30.1, 22.8. HRMS: calculated: *m/z* = 312.10305; found: *m/z* = 312.10410.

3-(5-Phenyl-4-(4-(trifluoromethyl)phenyl)oxazol-2-yl)propanoic acid (20f). Yield: 71 mg (23%). R_f -Value: 0.51 (3/1; hexane / EtOAc +3% AcOH). ^{1}H-NMR (300 MHz, DMSO-d_6): δ = 12.31 (s, 1H, -COO*H*), 7.77 (ps, 4H, *Ph*-CF_3), 7.57-7.44 (m, 5H, *Ph*), 3.08 (t, 2H, J = 7.0 Hz, CH_2-COOH), 2.79 (t, 2H, J = 6.9 Hz, -CH_2-CH_2). ^{13}C-NMR (75 MHz, DMSO-d_6): δ = 173.0, 162.8, 145.84, 136.0, 132.7, 129.2, 129.0, 127.9, 127.6, 126.7, 125.6, 125.5, 30.1, 22.8. HRMS: calculated: *m/z* = 362.09985; found: *m/z* = 362.10073.

3-(4-(4-Cyanophenyl)-5-phenyloxazol-2-yl)propanoic acid (20g). Yield: 24 mg (15%). R_f -Value: 0.32 (3/1; Hex / EtOAc +3% AcOH). ^{1}H-NMR (300 MHz, DMSO-d_6): δ = 12.32 (s, 1H, -COO*H*), 7.86 (d, 2H, J = 8.6 Hz, *Ph*-CN-3*H*,5*H*), 7.73 (d, 2H, J = 8.6 Hz, *Ph*-CN-2*H*,6*H*), 7.57-7.46 (m, 5H, *Ph*), 3.07 (t, 2H, J = 6.9 Hz, CH_2-COOH), 2.78 (t, 2H, J = 6.9 Hz, -CH_2-CH_2).^{13}C-NMR (75 MHz, DMSO-d_6): δ = 173.0, 163.0, 146.4, 136.5, 132.6, 129.5, 129.1, 127.8, 127.6, 126.9, 118.6, 110.3, 30.1, 22.8. HRMS: calculated: *m/z* = 319.10772; found: *m/z* = 319.10820.

3-(4-(4-Chlorophenyl)-5-phenyloxazol-2-yl)propanoic acid (20h). Yield: 19 mg (34%). R_f-Value: 0.46 (3/1; Hex / EtOAc +3% AcOH). ^{1}H-NMR (300 MHz, DMSO-d_6): δ = 12.31 (br, 1H, -COO*H*), 7.59-7.39 (m, 9H, *Ph*, *Ph*-Cl), 3.06 (t, 2H, J = 7.1 Hz, -CH_2-COOH), 2.78 (t, 2H, J = 7.0 Hz, -CH_2-CH_2). ^{13}C-NMR (75 MHz, DMSO-d_6): δ = 173.0, 162.5, 144.9, 133.1, 132.5, 130.7, 128.9, 128.9, 128.7, 128.6, 128.4, 128.1, 126.4, 30.1, 22.8. HRMS: calculated: *m/z* = 328.07350; found: *m/z* = 328.07469.

3-(4-(4-Methoxyphenyl)-5-phenyloxazol-2-yl)propanoic acid (20i). Yield: 58 mg (16%). R_f -Value: 0.12 (3/1; Hex / EtOAc +3% AcOH). ^{1}H-NMR (300 MHz, DMSO-d_6): δ = 12.33 (s, 1H, -COO*H*), 7.55-7.36 (m, 7H, *Ph*, *Ph*-OCH_3-2*H*,6*H*), 6.99 (d, 2H, J = 8.5 Hz, *Ph*-OCH_3-3*H*,5*H*), 3.85

(s, 3H, -C*H*$_3$), 3.06 (t, 2H, J = 7.0 Hz, C*H*$_2$-COOH), 2.79 (t, 2H, J = 6.9 Hz, -C*H*$_2$-CH$_2$).^{13}C-NMR (75 MHz, DMSO-*d*$_6$): δ = 173.1, 162.1, 159.0, 143.6, 134.2, 128.9, 128.7, 128.6, 128.5, 126.01, 124.2, 114.0, 55.0, 30.2, 22.9. HRMS: calculated: *m/z* = 324.12303; found: *m/z* = 324.12406.

3-(4-(4-Chloro-3-(trifluoromethyl)phenyl)-5-phenyloxazol-2-yl)propanoic acid (20j). Yield: 52 mg (11%). R$_f$ -Value: 0.32 (3/1; Hex / EtOAc +3% AcOH). ^{1}H-NMR (300 MHz, DMSO-d$_6$): δ = 12.40 (s, 1H, -COO*H*), 8.01 (sd, 1H, J = 1.9 Hz, *Ph*-4Cl-3CF$_3$-2*H*), 7.88 (dd, 1H, J = 8.4 Hz, 1.9 Hz, *Ph*-4Cl-3CF$_3$-6*H*), 7.80 (d, 1H, J = 8.4 Hz, *Ph*-4Cl-3CF$_3$-5*H*), 7.63-7.51 (m, 5H, *Ph*), 3.13 (t, 2H, J = 6.8 Hz, C*H*$_2$-COOH), 2.84 (t, 2H, J = 6.8 Hz, -C*H*$_2$-CH$_2$). ^{13}C-NMR (75 MHz, DMSO-*d*$_6$): δ = 173.0, 162.9, 145.9, 132.1, 132.0, 131.7, 131.5, 129.5, 129.1, 127.7, 126.9, 30.1, 22.8. HRMS: calculated: *m/z* = 396.06088; found: *m/z* = 396.06074.

3-(4-(3,4-Dichlorophenyl)-5-phenyloxazol-2-yl)propanoic acid (20k). Yield: 68 mg (21%). R$_f$ -Value: 0.43 (3/1; Hex / EtOAc +3% AcOH). ^{1}H-NMR (300 MHz, DMSO-d$_6$): δ = 12.31 (s, 1H, -COO*H*), 7.74 (sd, 1H, J = 2.0 Hz, *Ph*-3,4-diCl-2*H*), 7.66 (d, 1H, J = 8.3 Hz, *Ph*-3,4-diCl-5*H*), 7.56-7.44 (m, 6H, *Ph*-3,4-diCl-6*H*, *Ph*), 3.06 (t, 2H, J = 7.0 Hz, C*H*$_2$-COOH), 2.78 (t, 2H, J = 6.9 Hz, -C*H*$_2$-CH$_2$). ^{13}C-NMR (75 MHz, DMSO-*d*$_6$): δ = 172.9, 162.7, 145.6, 132.5, 131.8, 131.3, 130.9, 130.4, 129.3, 129.0, 128.6, 127.8, 127.0, 126.7, 30.1, 22.8. HRMS: calculated: *m/z* = 362.03453; found: *m/z* = 362.03564.

3-(4-(2,4-Dichlorophenyl)-5-phenyloxazol-2-yl)propanoic acid (20l). Yield: 50 mg (25%). R$_f$ -Value: 0.36 (3/1; Hex / EtOAc +3% AcOH). ^{1}H-NMR (300 MHz, DMSO-d$_6$): δ = 12.30 (s, 1H, -COO*H*), 7.86 (sd, 1H, J = 1.0 Hz, *Ph*-2,4-diCl-3*H*), 7.62-7.58 (m, 2H, *Ph*-2,4-diCl-5*H*,6*H*), 7.45-7.26 (m, 5H, *Ph*), 3.04 (t, 2H, J = 7.0 Hz, C*H*$_2$-COOH), 2.78 (t, 2H, J = 7.0 Hz, -C*H*$_2$-CH$_2$). ^{13}C-NMR (75 MHz, DMSO-*d*$_6$): δ = 172.9, 163.2, 140.6, 136.2, 135.5, 134.3, 133.5, 130.9, 129.8,

128.53, 128.5, 128.0, 127.9, 127.4, 126.9, 126.0, 30.2, 22.8. HRMS: calculated: *m/z* = 362.03453; found: *m/z* = 362.03563.

3-(4-(3,5-Dichlorophenyl)-5-phenyloxazol-2-yl)propanoic acid (20m). Yield: 23 mg (11%). R_f -Value: 0.35 (3/1; Hex / EtOAc +3% AcOH). ^{1}H-NMR (300 MHz, DMSO-d_6): δ = 12.31 (s, 1H, -COO*H*), 7.61-7.48 (m, 8H, *Ph*, *Ph*-3,5-diCl), 3.07 (t, 2H, J = 6.8 Hz, CH_2-COOH), 2.76 (t, 2H, J = 6.8 Hz, -CH_2-CH_2). ^{13}C-NMR (75 MHz, DMSO-d_6): δ = 173.0, 162.9, 146.1, 135.3, 134.3, 131.4, 129.6, 129.1, 127.6, 127.4, 126.9, 125.3, 30.1, 22.8. HRMS: calculated: *m/z* = 362.03453; found: *m/z* = 362.03575.

3-(4-(3,4-Dichlorophenyl)-5-phenyloxazol-2-yl)acrylic acid (22a, isomeric mixture). Instead of succinic acid maleic acid was used. Yield: 112 mg (yellow solid; 21%). R_f -Value: 0.56 (2/1; Hex / EtOAc +3% AcOH). ^{1}H-NMR (300 MHz, DMSO-d_6): δ = 7.88 (sd, 1H, J = 2.0 Hz, *Ph*-3,4-diCl-2*H*), 7.78 (sd, 0.4H, J = 2.0 Hz, *Ph*-3,4-diCl-2*H*), 7.69 (d, 1H, J = 8.4 Hz, *Ph*-3,4-diCl-5*H*), 7.69 (d, 1H, J = 8.4 Hz, *Ph*-3,4-diCl-5*H*), 7.67 (d, 0.4H, J = 8.4 Hz, *Ph*-3,4-diCl-5*H*), 7.65-7.45 (m, 9H, 2x*Ph*, 2x *Ph*-3,4-diCl-6*H*), 7.32 (d, 1.4H, J = 15.9 Hz, -C*H*=CH-), 6.87 (d, 1H, J = 15.9 Hz, =CH-COO*H*), 6.77 (d, 0.4H, J = 15.9 Hz, =CH-COO*H*). ^{13}C-NMR (75 MHz, DMSO-d_6): δ = 166.2, 166.2, 157.7, 157.5, 147.3, 143.8, 138.3, 134.5, 131.9, 131.9, 131.8, 131.5, 131.2, 131.1, 131.1, 130.8, 130.0, 129.2, 129.1, 129.0, 128.0, 128.0, 127.8, 127.5, 127.2, 127.1, 127.0, 126.7, 126.3. HRMS: calculated: *m/z* = 360.01888; found: *m/z* = 360.01937.

4-(4-(3,4-Dichlorophenyl)-5-phenyloxazol-2-yl)butanoic acid (22b). Instead of succinic acid glutaric acid was used. Yield: 121 mg (27%). R_f -Value: 0.57 (2/1; Hex / EtOAc +3% AcOH). ^{1}H-NMR (300 MHz, DMSO-d_6): δ = 12.40 (s, 1H, -COO*H*), 7.75 (sd, 1H, J = 1.9 Hz, *Ph*-3,4-diCl-2*H*), 7.66 (d, 1H, J = 8.4 Hz, *Ph*-3,4-diCl-5*H*), 7.56-7.44 (m, 6H, *Ph*, *Ph*-3,4-diCl-6*H*), 2.87 (t, 2H, J = 7.5 Hz, CH_2-COOH), 2.39 (t, 2H, J = 7.1 Hz, oxazole-CH_2-CH_2), 1.98 (q, 2H, J = 7.5 Hz,

-CH_2-C*H*$_2$-CH_2). ^{13}C-NMR (75 MHz, DMSO-*d*$_6$): δ = 174.0, 163.2, 145.7, 132.6, 131.9, 131.4, 131.0, 130.4, 129.4, 129.1, 128.7 127.9, 127.1, 126.8, 32.6, 26.5, 21.69. HRMS: calculated: *m/z* = 376.05018; found: *m/z* = 376.05145.

2-(4-(3,4-Dichlorophenyl)-5-phenyloxazol-2-yl)benzoic acid (22c). Instead of succinic acid phthalic acid was used. Yield: 70 mg (pale yellow solid; 14%). R_f -Value: 0.56 (2/1; Hex / EtOAc +3% AcOH). ^{1}H-NMR (300 MHz, DMSO-d_6): δ = 13.40 (s, 1H, -COO*H*), 8.00 (dd, 1H, J = 6.8 Hz, 1.9 Hz, *Ph*-3,4-diCl-6*H*), 7.85 (sd, 1H, J = 1.9 Hz, *Ph*-3,4-diCl-2*H*), 7.78-7.57 (m, 7H, *Ph*-COOH, *Ph*-3*H*,5*H*, *Ph*-3,4-diCl-6*H*), 7.54-7.47 (m, 3H, *Ph*-2*H*,4*H*,6*H*). ^{13}C-NMR (75 MHz, DMSO-*d*$_6$): δ = 169.1, 159.3, 146.8, 133.4, 133.3, 132.4, 131.6, 131.1, 130.9, 130.9, 129.7, 129.3, 129.2, 128.9, 127.6, 127.3, 126.9, 124.8. HRMS: calculated: *m/z* = 410.03453; found: *m/z* = 410.03509.

3-(4-(3,4-Dichlorophenyl)-5-phenyloxazol-2-yl)benzoic acid (22d). Instead of succinic acid isophthalic acid was used. Yield: 53 mg (11%). R_f -Value: 0.48 (2/1; Hex / EtOAc +3% AcOH). ^{1}H-NMR (300 MHz, DMSO-d_6): 13.40 (bs, 1H, -COO*H*), 8.60 (t, 1H, J = 1.4 Hz, *Ph*-COOH-5*H*), 8.35-8.32 (m, 2H, *Ph*-COOH-2*H*,4*H*), 8.13-8.09 (m, 1H, *Ph*-COOH-6*H*), 7.88 (sd, 1H, 2.0 Hz, *Ph*-Cl-2*H*), 7.75-7.69 (m, 4H, *Ph*-Cl-5*H, Ph*-2*H*,4*H*,6*H*), 7.62 (dd, 1H, J = 8.4 Hz, 2.0 Hz, *Ph*-Cl-6*H*). ^{13}C-NMR (75 MHz, DMSO-*d*$_6$): δ = 166.1, 159.0, 146.7, 133.7, 132.4, 131.8, 131.6, 131.1, 131.0, 130.3, 129.9, 129.8, 129.3, 129.1, 127.5, 127.5, 127.1, 126.7, 126.6. HRMS: calculated: *m/z* = 410.03453; found: *m/z* = 410.03460.

4-(4-(3,4-Dichlorophenyl)-5-phenyloxazol-2-yl)benzoic acid (22e). Instead of succinic acid terephthalic acid was used. Yield: 57 mg (pale yellow solid; 12%). R_f -Value: 0.53 (2/1; Hex / EtOAc +3% AcOH). ^{1}H-NMR (300 MHz, DMSO-d_6): δ = 13.29 (bs, 1H, -COO*H*), 8.26-8.20 (m, 2H, *Ph*-COOH-3*H*,5*H*), 8.12-8.10 (m, 2H, *Ph*-COOH-2*H*,6*H*), 7.91 (dd, 1H, J = 8.7 Hz, 1.8 Hz,

Ph-3,4-diCl-6*H*), 7.75-7.65 (m, 3H, *Ph*-3,4-diCl-2*H, Ph*-3*H*,5*H*), 7.62-7.77 (m, 1H, *Ph*-3,4-diCl-5*H*), 7.53-7.46 (m, 3H, *Ph*-2*H*,4*H*,6*H*). ^{13}C-NMR (75 MHz, DMSO-d_6): δ = 166.7, 159.2, 143.5, 137.9, 132.7, 132.3, 131.9, 131.6, 131.2, 130.1, 129.7, 129.2, 129.0, 128.4, 127.9, 127.5, 127.0, 126.5, 126.3, 126.3. HRMS: calculated: *m/z* = 410.03453; found: *m/z* = 410.03478.

5-(2-(3,4-Dichlorophenyl)-2-oxoethoxy)-5-oxopentanoic acid (24). To a solution of 3.3 g glutaric acid **21b** (24.6 mmol, 3 equiv) in 150 mL acetone was added 3.5 mL triethylamine (24.6 mmol, 3 equiv) and stirred at room temperature. After 30 minutes 2.3 g (8.2 mmol, 1 equiv) 3,4-dichlorophenylacylbromide **23** was added in small portions and the reaction monitored by TLC. The mixture was concentrated under reduced pressure and taken up in 50 mL 1 N hydrochloric acid following extraction with dichloromethane. The solvent was dried over $MgSO_4$, removed under reduced pressure and the residue purified via column chromatography (eluent: 98/2; DCM / MeOH +1% AcOH) yielding 2.69 g tan solid (97%). R_f-Value: 0.20 (7/3; Hex / EtOAc +0.1% AcOH). ^{1}H-NMR (250 MHz, $CDCl_3$): δ = 8.01 (sd, 1H, J = 2.0 Hz, *Ph*-2*H*), 7.74 (dd, 1H, J = 8.4 Hz, 2.0 Hz, *Ph*-6*H*), 7.59 (d, 1H, J = 8.2 Hz, *Ph*-5*H*), 5.29 (s, 2H, C(O)-CH_2-O), 2.57 (dt, 4H J = 18.3 Hz, 7.2 Hz, 2x C(O)-CH_2-CH_2-), 2.06 (quin, 2H, J = 7.1 Hz, CH_2-CH_2-CH_2). ESI-MS: *m/z* = 316.9 $[M\text{-}2H^+]^-$.

4-(4-(3,4-Dichlorophenyl)oxazol-2-yl)butanoic acid (25). 1.2 g **24** (3.7 mmol, 1 equiv), 1.1 g acetamide (18.5 mmol, 5 equiv) and 0.5 mL boron trifluoride diethyl etherate (3.7 mmol, 1 equiv) were mixed under neat conditions for 30 hours at 140 °C. The mixture was poured into 50 mL 1 N hydrochloric acid following extraction with ethyl acetate. The combined organic phases were washed with brine, dried over $MgSO_4$ and removed under reduced pressure. The residue was purified via column chromatography (eluent: 4/1; Hex/acetone) yielding 0.64 g brown solid (58%). R_f-Value: 0.20 (7/3; Hex / EtOAc +0.1% AcOH). ^{1}H-NMR (250 MHz, DMSO-d_6): δ = 12.13 (bs,

1H, -O*H*), 8.63 (s, 1H, oxazolyl-5*H*), 7.99 (sd, 1H, J = 1.9 Hz, *Ph*-2*H*), 7.77-7.66 (m, 2H, *Ph*-5*H*,6*H*), 2.83 (t, 2H, J = 7.5 Hz, -CH_2-C(O)), 2.35 (t, 2H, J = 7.3 Hz, oxazole-CH_2-), 1.94 (quin, 2H, J = 7.4 Hz, CH_2-CH_2-CH_2). ^{13}C-NMR (75 MHz, DMSO-d_6): δ = 178.3, 164.7, 138.6, 134.0, 133.0, 131.7, 131.0, 130.7, 127.3, 124.6, 32.9, 27.2, 21.8. HRMS: calculated: *m/z* = 300.01888; found: *m/z* = 300.01896.

4-(5-Bromo-4-(3,4-dichlorophenyl)oxazol-2-yl)butanoic acid (26). To a solution of 0.7 g **25** (2.3 mmol, 1.0 equiv) and 0.2 g ammonium acetate (0.2 mmol, 0.1 equiv) in 20 mL acetonitrile was added 0.4 g NBS (2.4 mmol, 1.05 equiv) in small portions. The mixture was stirred for 1.5 hours at room temperature, the solvent removed under reduced pressure and the residue suspended in 100 mL water. The solidified product was isolated by filtration and purified via column chromatography (eluent: 7/3; Hex / EtOAc +1% AcOH) yielding 0.58 g title compound (67%). R_f-Value: 0.29 (7/3; Hex / EtOAc +0.1% AcOH). ^{1}H-NMR (300 MHz, DMSO-d_6): δ = 7.97 (sd, 1H, J = 2.0 Hz, *Ph*-2*H*), 7.82 (dd, 1H, J = 8.5 Hz, 2.1 Hz, *Ph*-6*H*), 7.71 (d, 1H, J = 8.5 Hz, *Ph*-5*H*), 2.81 (t, 2H, J = 7.5 Hz, -CH_2-C(O)), 2.34 (t, 2H, J = 7.2 Hz, oxazole-CH_2-), 1.91 (quin, 2H, J = 7.4 Hz, CH_2-CH_2-CH_2). ^{13}C-NMR (75 MHz, DMSO-d_6): δ = 174.4, 165.9, 134.0, 132.0, 131.5, 131.2, 130.6, 127.6, 126.1, 118.0, 32.9, 27.0, 21.8. HRMS: calculated: *m/z* = 379.92734; found: *m/z* = 379.92693.

General procedure for the synthesis of oxaprozin-derivatives 28a-k. A vial filled with 127 mg K_3PO_4, 2 mL water and 1 mL DMF was capped and degassed with argon using an ultrasonic bath. Afterwards 23 mg tetrakis(triphenylphosphine)palladium(0) (0.02 mmol, 0.1 equiv), 76 mg of title compound **26** (0.2 mmol, 1.0 equiv) and the appropriate boronic acid derivative **27a-k** (0.2 mmol, 1.0 equiv) were added to the solution. The resulting mixture was degassed again and heated to 80 °C for 48 hours. The mixture was diluted with 20 mL EtOAc and

filtrated over silica gel. After rinsing the silica gel several times with EtOAc, the solution was washed with 1 N hydrochloric acid, brine, dried over $MgSO_4$ and concentrated under reduced pressure. The residue was purified via preparative HPLC.

4-(4-(3,4-Dichlorophenyl)-5-(pyridin-4-yl)oxazol-2-yl)butanoic acid (28a). Pyridin-4-ylboronic acid **27a** was used as coupling agent. Yield: 2 mg (3%). R_f -Value: 0.21 (98/2; DCM / MeOH +0.1% AcOH). ^{1}H-NMR (300 MHz, DMSO-d_6): δ = 8.64 (d, 2H, J = 6.1 Hz, *pyridinyl*-3*H*,5*H*), 7.82 (sd, 1H, J = 2.0 Hz, *Ph*-2*H*), 7.73 (d, 1H, J = 8.4 Hz, *Ph*-5*H*), 7.56 (dd, 1H, J = 8.4 Hz, 2.0 Hz, *Ph*-6*H*), 7.45-7.53 (m, 2H, *pyridinyl*-2*H*,6*H*), 2.91 (t, 2H, J = 7.5 Hz, -CH_2-C(O)), 2.39 (t, 2H, J = 7.1 Hz, oxazole-CH_2-), 1.99 (quin, 2H, J = 7.4 Hz, CH_2-CH_2-CH_2). ^{13}C-NMR (75 MHz, DMSO-d_6): δ = 164.6, 150.5, 143.0, 140.7, 139.2, 137.8, 135.3, 134.9, 132.1, 131.7, 131.4, 131.2, 129.6, 127.9, 119.9, 32.8, 26.6, 21.7. HRMS: calculated: *m/z* = 377.04542; found: *m/z* = 377.04579.

4-(4-(3,4-Dichlorophenyl)-5-(pyridin-3-yl)oxazol-2-yl)butanoic acid (28b). Pyridin-3-ylboronic acid **27b** was used as coupling agent. Yield: 8 mg (11%). R_f -Value: 0.26 (98/2; DCM / MeOH +0.1% AcOH). ^{1}H-NMR (300 MHz, DMSO-d_6): δ = 8.74 (sdd, 1H, J = 2.2 Hz, 0.7 Hz, *pyridinyl*-2*H*), 8.63 (dd, 1H, J = 4.8 Hz, 1.6 Hz, *pyridinyl*-4*H*), 7.91-8.01 (m, 1H, *pyridinyl*-6*H*), 7.77 (sd, 1H, J = 2.0 Hz, *Ph*-2*H*), 7.68 (d, 1H, J = 8.4 Hz, *Ph*-5*H*), 7.46-7.55 (m, 2H, *Ph*-6*H*, *pyridinyl*-5*H*), 2.90 (t, 2H, J = 7.5 Hz, -CH_2-C(O)), 2.40 (t, 2H, J = 7.2 Hz, oxazole-CH_2-), 1.92-2.08 (m, 2H, CH_2-CH_2-CH_2). ^{13}C-NMR (75 MHz, DMSO-d_6): δ = 174.0, 164.1, 150.0, 147.4, 143.1, 134.4, 133.4, 132.2, 131.6, 131.2, 130.9, 128.9, 127.2, 124.4, 124.1, 32.7, 26.6, 21.7. HRMS: calculated: *m/z* = 377.04542; found: *m/z* = 377.04623.

4-(4-(3,4-Dichlorophenyl)-5-(2-fluorophenyl)oxazol-2-yl)butanoic acid (28c). (2-Fluorophenyl)boronic acid **27c** was used as coupling agent. Yield: 14 mg (18%). R_f -Value: 0.42

(3/2; Hex / EtOAc +0.1% AcOH). ^{1}H-NMR (300 MHz, DMSO-d_6): δ = 7.64 (sd, 1H, J = 1.5 Hz, *Ph*-3,4-diCl-2*H*), 7.45-7.07 (m, 6H, *Ph*-3,4-diCl-5*H*,6*H*, *Ph*-2-F), 2.89 (t, 2H, J = 7.4 Hz, -CH_2-C(O)), 2.48 (t, 2H, J = 6.9 Hz, oxazole-CH_2-), 2.12 (quin, 2H, J = 7.3 Hz, CH_2-CH_2-CH_2). ^{13}C-NMR (75 MHz, DMSO-d_6): δ = 178.1, 163.9, 161.1, 157.7, 140.7, 134.9, 132.6, 131.8, 131.5, 130.5, 130.3, 128.8, 126.0, 124.6, 116.7, 116.4, 32.9, 27.2, 21.80. HRMS: calculated: *m/z* = 394.04075; found: *m/z* = 394.04059.

4-(4-(3,4-Dichlorophenyl)-5-(2,5-difluorophenyl)oxazol-2-yl)butanoic acid (28d). (2,5-Difluorophenyl)boronic acid **27d** was used as coupling agent. Yield: 22 mg (27%). R_f -Value: 0.53 (3/2; Hex / EtOAc +0.1% AcOH). ^{1}H-NMR (300 MHz, DMSO-d_6): δ = 7.70 (sd, 1H, J = 2.0 Hz, *Ph*-3,4-diCl-2*H*), 7.64 (d, 1H, J = 8.4 Hz, *Ph*-3,4-diCl-5*H*), 7.50-7.59 (m, 1H, *Ph*-3,4-diCl-6*H*), 7.33-7.49 (m, 3H, *Ph*-2,5-diF), 2.89 (t, 2H, J = 7.5 Hz, -CH_2-C(O)), 2.40 (t, 2H, J = 7.3 Hz, oxazole-CH_2-), 1.99 (quin, 2H, J = 7.4 Hz, CH_2-CH_2-CH_2). ^{13}C-NMR (75 MHz, DMSO-d_6): δ = 174.0, 164.6, 159.8, 156.6, 153.4, 138.9, 134.6, 132.0, 131.4, 130.9, 130.7, 128.1, 126.5, 119.0, 116.8, 32.7, 26.6, 21.7. HRMS: calculated: *m/z* = 412.03133; found: *m/z* = 412.03118.

4-(4-(3,4-Dichlorophenyl)-5-(3-fluorophenyl)oxazol-2-yl)butanoic acid (28e). (3-Fluorophenyl)boronic acid **27e** was used as coupling agent. Yield: 31 mg (40%). R_f -Value: 0.44 (3/2; Hex / EtOAc +0.1% AcOH). ^{1}H-NMR (300 MHz, DMSO-d_6): δ = 12.19 (s, 1H, -COO*H*), 7.78 (sd, 1H, J = 2.0 Hz, *Ph*-3,4-diCl-2*H*), 7.69 (d, 1H, J = 8.4 Hz, *Ph*-3,4-diCl-5*H*), 7.47-7.58 (m, 2H, *Ph*-3,4diCl-6*H*, *Ph*-3-F-2*H*), 7.38 (pd, 2H, J = 7.4 Hz, *Ph*-3-F-4*H*,6*H*) 7.22-7.34 (m, 1H, *Ph*-3-F-5*H*), 2.88 (t, 2H, J = 7.5 Hz, -CH_2-C(O)), 2.40 (t, 2H, J = 7.2 Hz, oxazole-CH_2-), 1.99 (quin, 2H, J = 7.3 Hz, CH_2-CH_2-CH_2). ^{13}C-NMR (75 MHz, DMSO-d_6): δ = 178.2, 164.5, 163.4, 161.2, 144.9, 133.5, 132.9, 132.4, 131.9, 130.6, 130.1, 129.8, 127.0, 122.1, 115.9, 113.6, 32.9, 27.1, 21.8. HRMS: calculated: *m/z* = 394.04075; found: *m/z* = 394.03928.

4-(4-(3,4-Dichlorophenyl)-5-(3-methoxyphenyl)oxazol-2-yl)butanoic acid (28f). (3-Methoxyphenyl)boronic acid **27f** was used as coupling agent. Yield: 41 mg (50%). R_f-Value: 0.24 (7/3; Hex / EtOAc +0.1% AcOH). ^{1}H-NMR (300 MHz, DMSO-d_6): δ = 7.77 (sd, 1H, J = 2.0 Hz, , *Ph*-3,4-diCl-2*H*), 7.65 (d, 1H, J = 8.4 Hz, *Ph*-3,4-diCl-5*H*), 7.52 (dd, 1H, J = 8.4 Hz, 2.0 Hz, *Ph*-3,4-diCl-6*H*), 7.38 (t, 1H, J = 7.7 Hz, *Ph*-3-CH_3-5*H*), 6.96-7.14 (m, 3 H, *Ph*-3-CH_3-2*H*,4*H*,6*H*), 3.74 (s, 3H, -C*H*$_3$), 2.86 (t, 2H, J = 7.5 Hz, , -C*H*$_2$-C(O)), 2.39 (t, 2H, J = 7.2 Hz, oxazole-C*H*$_2$-), 1.98 (quin, 2H, J = 7.3 Hz, CH_2-C*H*$_2$-CH_2). ^{13}C-NMR (75 MHz, DMSO-*d*$_6$): δ = 174.0, 163.2, 159.5, 145.5, 132.7, 132.1, 131.4, 130.9, 130.5, 130.4, 129.1, 128.9, 127.3, 119.1, 115.2, 112.0, 55.2, 32.8, 26.6, 21.8. HRMS: calculated: *m/z* = 406.06074; found: *m/z* = 406.06096.

4-(5-(3-Cyanophenyl)-4-(3,4-dichlorophenyl)oxazol-2-yl)butanoic acid (28g). (3-Cyanophenyl)boronic acid **27g** was used as coupling agent. Yield: 32 mg (40%). R_f-Value: 0.17 (7/3; Hex / EtOAc +0.1% AcOH). ^{1}H-NMR (300 MHz, DMSO-d_6): δ = 8.01 (s, 1H, *Ph*-3,4-diCl-2*H*), 7.84 (d, 1H, J = 8.1 Hz, *Ph*-3,4-diCl-5*H*), 7.89 (d, 1H, J = 7.7 Hz, *Ph*-3,4-diCl-6*H*), 7.76 (st, 1H, J = 1.9 Hz, *Ph*-3-CN-2*H*), 7.60-7.72 (m, 2H, *Ph*-3-CN-4*H*,5*H*), 7.49 (dd, 1H, J = 8.4 Hz, 2.0 Hz, *Ph*-3-CN-6*H*), 2.89 (t, 2H, J = 7.5 Hz, -C*H*$_2$-C(O)), 2.40 (t, 2H, J = 7.2 Hz, oxazole-C*H*$_2$-), 2.00 (quin, 2H, J = 7.3 Hz, CH_2-C*H*$_2$-CH_2). ^{13}C-NMR (75 MHz, DMSO-*d*$_6$): δ = 174.0, 163.9, 143.6, 133.4, 132.7, 132.1, 131.6, 131.2, 131.1, 131.0, 130.4, 130.1, 129.2, 129.0, 127.3, 118.1, 112.4, 32.7, 26.6, 21.7. HRMS: calculated: *m/z* = 401.04542; found: *m/z* = 401.04548.

4-(4-(3,4-Dichlorophenyl)-5-(3-(trifluoromethyl)phenyl)oxazol-2-yl)butanoic acid (28h). (3-(Trifluoromethyl)phenyl)boronic acid **27h** was used as coupling agent. Yield: 11 mg (12%). R_f-Value: 0.51 (3/2; Hex / EtOAc +0.1% AcOH). ^{1}H-NMR (300 MHz, DMSO-d_6): δ = 7.86-7.77 (m, 4H, *Ph*-3,4-diCl, *Ph*-3-CF_3-6*H*), 7.73-7.67 (m, 2H, *Ph*-3-CF_3-2*H*,5*H*), 7.52 (dd, 1H, J = 8.4 Hz, J = 2 Hz, *Ph*-3-CF_3-4*H*), 2.90 (t, 2H, J = 7.4 Hz, -C*H*$_2$-C(O)), 2.40 (t, 2H, J = 7.2 Hz,

oxazole-C*H*$_2$-), 1.99 (quin, 2H, J = 7.4 Hz, CH$_2$-C*H*$_2$-CH$_2$). ^{13}C-NMR (125 MHz, DMSO-*d*$_6$): δ = 173.8, 163.6, 143.8, 133.0, 132.0, 131.3, 130.8, 130.7, 130.3, 130.2, 129.7, 129.5, 128.7, 127.2, 125.5, 124.6, 122.8, 32.5, 26.3, 21.5. HRMS: calculated: *m/z* = 444.03756; found: *m/z* = 444.03752.

4-(4-(3,4-Dichlorophenyl)-5-(*m*-tolyl)oxazol-2-yl)butanoic acid (28i). *m*-Tolylboronic acid **27i** was used as coupling agent. Yield: 17 mg (21%). R$_f$ -Value: 0.16 (98/2; DCM / MeOH +0.1% AcOH). ^{1}H-NMR (300 MHz, DMSO-d$_6$): δ = 7.76 (sd, 1H, J = 2.0 Hz, *Ph*-3,4-diCl-2*H*), 7.64 (d, 1H, J = 8.4 Hz, *Ph*-3,4-diCl-5*H*), 7.51 (dd, 1H, J = 8.4 Hz, 2.0 Hz, *Ph*-3,4-diCl-6*H*), 7.22-7.41 (m, 4H, *Ph*-3-CH$_3$), 2.86 (t, 2H, J = 7.5 Hz, -C*H*$_2$-C(O)), 2.39 (t, 2H, J = 7.2 Hz, oxazole-C*H*$_2$-), 2.32 (s, 3H, -C*H*$_3$), 1.98 (quin, 2H, J = 7.4 Hz, CH$_2$-C*H*$_2$-CH$_2$). ^{13}C-NMR (75 MHz, DMSO-*d*$_6$): δ = 173.9, 163.2, 145.9, 138.5, 132.7, 131.8, 131.4, 130.9, 130.4, 130.0, 129.0, 128.6, 127.9, 127.3, 127.0, 124.0, 32.7, 26.6, 21.8, 20.9. HRMS: calculated: *m/z* = 390.06583; found: *m/z* = 390.06567.

4-(4-(3,4-Dichlorophenyl)-5-(3-ethynylphenyl)oxazol-2-yl)butanoic acid (28j). (3-Ethynylphenyl)boronic acid **27j** was used as coupling agent. Yield: 8 mg (10%). R$_f$ -Value: 0.30 (7/3; Hex / EtOAc +0.1% AcOH). ^{1}H-NMR (300 MHz, DMSO-d$_6$): δ = 7.79 (sd, 1H, J = 2.0 Hz, *Ph*-3,4-diCl-2*H*), 7.46-7.73 (m, 6H, *Ph*-3,4-diCl-5*H*,6*H*, *Ph*-3- C≡CH), 4.30 (s, 1H, C≡C*H*), 2.90 (t, 2H, J = 7.5 Hz, -C*H*$_2$-C(O)), 2.41 (t, 2H, J = 7.2 Hz, oxazole-C*H*$_2$-), 2.01 (quin, 2H, J = 7.3 Hz, CH$_2$-C*H*$_2$-CH$_2$). ^{13}C-NMR (75 MHz, DMSO-*d*$_6$): δ = 174.0, 163.6, 144.6, 132.6, 132.4, 132.3, 131.8, 131.6, 131.5, 131.0, 128.9, 128.7, 128.5, 127.3, 127.2, 122.6, 82.5, 81.8, 32.7, 26.6, 21.7. HRMS: calculated: *m/z* = 400.05018; found: *m/z* = 400.05005.

4-(5-(3-Chlorophenyl)-4-(3,4-dichlorophenyl)oxazol-2-yl)butanoic acid (28k). (3-Chlorophenyl)boronic acid **27k** was used as coupling agent. Yield: 4 mg (5%). R$_f$ -Value: 0.47 (3/2; Hex / EtOAc +0.1% AcOH). ^{1}H-NMR (300 MHz, DMSO-d$_6$): δ = 7.78 (sd, 1H, J = 2.0 Hz,

Ph-3,4-diCl-2*H*), 7.69 (d, 1H, J = 8.4 Hz, *Ph*-3,4-diCl-5*H*), 7.58-7.63 (m, 1H, *Ph*-3,4-diCl-6*H*), 7.47-7.54 (m, 4H, *Ph*-3-Cl), 2.88 (t, 2H, J = 7.4 Hz, -CH_2-C(O)), 2.39 (t, 2H, J = 7.2 Hz, oxazole-CH_2-), 1.99 (quin, 2H, J = 7.3 Hz, CH_2-CH_2-CH_2).^{13}C-NMR (125 MHz, DMSO-d_6): δ = 174.0, 163.7, 144.2, 133.8, 133.0, 132.4, 131.6, 131.1, 130.8, 129.9, 129.1, 129.0, 127.4, 126.3, 125.3, 39.9, 32.7, 26.6, 21.7. HRMS: calculated: *m/z* = 410.01120; found: *m/z* = 410.01126.

Cloning of the N-terminal sEH domain

The cloning of the construct, encoding the aa1-222 of the sEH with a hexa-His-tag at the N-terminus as well as a thrombin cleavage site followed by a second hexa-His-tag at the C-terminus, was published previously[16] and was used for activity assays.

For the crystallization, DSF and ITC experiments a new construct was created. The sEH-P sequence covering the aa2-224 of the sEH was amplified by PCR (forward primer ccccGGTACCCTGCGCGCGGCCGTCTTCG, reverse primer CCCCCTCGAGTTAGGTATTGAGAAGCTGGATTCCGG) from the sEH full length construct published by Hahn et al.[24]. The PCR product was cloned into a pET29b derivative (in which the expressed ORF was changed to the one from pBH4 with TEV side) using KpnI and XhoI. The target protein is expressed as fusion protein with an N-terminal 6x His-tag followed by a TEV recognition and cleavage side. The plasmid carries a kanamycin resistance gene.

Protein Expression and Purification

The sEH-P for activity assays as well as the sEH-H used in the performed activity assays and DSF experiments was expressed and purified as published previously by Klingler et. al.[16] and

Lukin et. al[25]. The proteins for the assay were flash frozen in liquid nitrogen after the addition of 20% (v/v) glycerol and stored at -80°C.

The expression of the sEH-P for crystallization, DSF and ITC experiments was done according to previously published expression full length sEH[24], while for the purification a modified protocol was used. In brief, 10 mL pre-culture of the BL21(DE3) cells, co-transformed with the sEH-P plasmid as well as a co-plasmid for the expression for rare codon tRNAs, were used to inoculate a 1 L culture of autoinduction media ZYP5052[26] supplemented with chloramphenicol (35 µg/mL) as well as kanamycin (100 µg/mL). The cultures were incubated at 37 °C and 180 rpm for 3-4 h, before the temperature was reduced to 16 °C. The cultures were harvested after 36 h by centrifugation (5,554 x g, 4 °C, 20 min). The resulting pellets were stored at -20 °C or directly processed. For ITC measurements expression pellets were resuspended in buffer A (50 mM Bis Tris pH 7,2 (HCl), 500 mM NaCl, 5 mM β-ME, 5% (v/v) Glycerol, 20 mM Imidazole pH 7 (HCl)) with one tablet of Complete EDTA free protease inhibitor mix (Roche, Basel, Switzerland) and a trace amount of DNAse I (Applichem, Darmstadt, Germany) before purified as follows. After passing 20 x through an Invensys APV-1000 Homogenizer (APV System, Denmark) the resulting solution was subsequently centrifuged at 43.992 X g for 60 min at 4°C to pellet debris. The supernatant was filtrated through a 0.45 µm syringe filter before loading onto a 5-mL HisTrap HP (GE Healthcare, Solingen, Germany) column pre-equilibrated with buffer A. The column was washed with 1% (v/v) of buffer B (buffer A with 400 mM instead of 20 mM Imidazole pH 7 (HCl)) before the protein was eluted at 50% (v/v) buffer B. The protein fraction was concentrated to a final volume of 5 mL using a Centriprep YM-3 with a molecular weight cutoff of 3.000 Da (Millipore, Germany), filtrated through a 0.45 µm syringe filter and applied onto a Superdex 200 HiLoad 16/600 column (GE Healthcare, Germany) equilibrated and run at 1 ml/min in phosphatse

assay buffer (50 mM acetate, 10 mM $MgCl_2$, pH 5.75 (HCl)) supplemented with an additional 5% (v/v) glycerol. The concentration of the protein for ITC measurements was determined by absorption measurement with the Nanodrop spectrophotometer (Implen, Muenchen, Germany).

For crystallization expression pellets were resuspended in buffer C (50 mM Bis Tris pH 7,2 (HCl), 500 mM NaCl, 1 mM TCEP, 5% (v/v) Glycerol) with 18 µL Protease Inhibitor Mix. Cells were lysed by sonification before 3 mL 5% PEI pH 7.5 (HCl) solution was added to 100 mL cell solution and subsequently centrifuged to pellet debris. The supernatant was loaded onto 5 mL of cobalt beads (GE Healthcare, self loaded with Co) preequilibrated with buffer C. The beads were subsequently washed with of buffer C supplemented with 20 mM, 40 mM, 60 mM and 250 mM Imidazole pH7 (HCl). The protein mainly eluted at the 60/ 250 mM wash-fractions. These fractions were concentrated (Amicon® Ultra Centrifugal Filters, 3,000 MWCO, Merck Millipore) to a final volume of 5 mL and filtrated by a 0.45 µm syringe filter before the sample was loaded on a Superdex 200 HiLoad 16/600 column (GE Healthcare, Germany) equilibrated and run with crystallization buffer (20 mM Tris, 100 mM NaCl, 0,5 mM TCEP, pH 7.5 (HCl)) The concentration of the Protein was determined by Nanodrop (Implen, Muenchen, Germany). The identity of the protein was verified by intact mass spectrometry (data not shown).

The full length human, mouse and rat sEH were expressed in a baculovrius/insect cell system and purified by affinity as described previously[27]. The concentrated purified enzymes appeared as a single band on SDS-PAGE separation and Coomassie Brilliant Blue staining with an estimated purity above 95%. The final preparations had no detectable esterase or glutathione S-transferase activity[28].

FDP based Phosphatase assay

The fluorescein diphosphate (FDP) assay was performed as published previously by Klingler et al.[16] using frozen sEH-P, as well as human, rat, and murine full length sEH. In brief, the assay was performed in a black 96-well microplate where 1 µL compound in DMSO (or DMSO only, in case of the positive control) was mixed with 89 µL of protein solution (0.1 µM final concentration for sEH-P, 0.1 µM final concentration for human full length sEH and 0.1 µM final concentration for rat full length sEH and 0.01 µM final concentration for mouse full length sEH) in phosphatase assay buffer (50 mM acetate, 10 mM $MgCl_2$, pH 5.75) supplemented with 0.01% (w/v) Triton X-100). For the blank assay buffer without protein was used. The plates were incubated at RT for 30 mins to allow the binding of the inhibitor. To start the reaction, 10 µL FDP solution (10 µM final concentration) in assay buffer were added and the fluorescence changes (λ_{ex} = 485 nm, λ_{em} = 525 nm) were detected in 30 points over the duration of 30 mins using an infinite F200pro plate reader (Tecan, Crailsheim, Germany). All samples were measured in triplicates on the plate as well as in 3 separate experiments. The percent inhibition was calculated in comparison to activities of blank (without protein) and positive control wells (without inhibitor). To calculate IC_{50} values data obtained from measurements with at least six different inhibitor concentrations were fitted with a sigmoidal dose-response function using GraphPad Prism software (version 5.03; GraphPad Software, Inc.).

DiFMUP based Phosphatase assay

The 6,8-difluoro-4-methylumbelliferyl phosphate (DiFMUP) (Life technologies) assay was done to determine the K_m of DiFMUP as well as the K_i value of 22b for the sEH-P and human full length sEH. In brief, the assay was performed in a black 96-well microplate where different substrate concentrations (final concertation in 100 µL: 600, 400, 300, 200, 100, 30, 10, 3, 1, 0.3, 0.1, and

0 µM substrate dissolved in DMSO (or pure DMSO in case of 0 µM) and acetate buffer (50 mM acetate, 10 mM $MgCl_2$, pH 5.75) were mixed with a protein inhibitor solution (or pure DMSO in case of the control or K_m measurements). The solution contained protein (50 nM final concentration for sEH-P as well as for human full length sEH) in phosphatase assay buffer buffer (50 mM acetate, 10 mM $MgCl_2$, pH 5.75) supplemented with Triton X-100 to a final concentration of 0.01% (w/v) as well as different inhibitor concentrations (final concentrations of 22b 10, 3, 1, 0.3, 0.1, 0.03, 0.01 µM as well as pure DMSO). Protein inhibitor solutions were incubated at RT for 30 mins to allow the binding of the inhibitor before the reaction was started by adding it to the substrate mix in the plate. Total amount of DMSO in the assay volume was 3.5% (v/v). The fluorescence changes (λ_{ex} = 360 nm, λ_{em} = 465 nm) were detected in 45 points over the duration of 45 mins using an infinite F200pro plate reader (Tecan, Crailsheim, Germany). All conditions were measured as triplicate on the plate. The fluorescence changes in the linear phase of the reaction were determined by a linear fit, before mean and stander deviation were calculated in Microsoft Excel. Values of the different measurements were exported to GraphPad Prism (version 7.05; GraphPad Software, Inc.) and analyzed by a mixed model inhibition fit. The K_m value for the DiFMUP was determined form the data of the DMSO measurement using a Michealis Menten fit.

PHOME based Hydrolase Assay

The fluorescence-based sEH hydrolase activity assay was performed as described previously[25,29] in a 96- well format with some minor modifications.

In short, sEH (0.1 µM final concentration for all tested proteins) was dissolved in hydrolase assay buffer (Bis-Tris buffer, pH 7) supplemented with 0.1 mg/ml BSA as well as Triton-X 100 in a final concentration of 0.01%. 89 µl of protein solution were incubated with 1 µL of different

concentrations of compounds (final DMSO concentration 1%) for 30 min at room temperature. The reaction was started by 10 µl of a PHOME (3-phenyl-cyano-(6-methoxy-2-naphthalenyl)-methyl ester-2-oxirane-acetic acid) solution (to the final concentration 50 µM). The hydrolysis of the non-fluorescent substrate by the sEH to the fluorescent 6-methoxynaphtaldehyde is measured (λ_{ex} = 330 nm, λ_{em} = 465 nm) by a Tecan Infinite F200 Pro plate reader. The reaction was monitored over a duration of 45 min (one point every minute). A blank control (no protein and no compound) as well as a positive control (no compound) was carried out as well. All measurements were performed in triplicates.

Differential scanning experiments

Differential scanning fluorimetry (DSF)[30] was performed in a PCR-plate at a total volume of 40 µL. sEH-H and sEH-P (C_{final} = 5 µM), Triton X-100 (C_{final} = 0.001% (w/v)) and SYPRO Orange (Thermo Fisher Scientific GmbH, Braunschweig Germany) (C_{final} = 2.5x) were either mixed with phosphatase assay buffer (50 mM acetate, 10 mM $MgCl_2$, pH 5.75) or hydrolase assay buffer (Bis-Tris buffer, pH 7), and the corresponding inhibitors. All inhibitors were tested at a fix concentration of 50 µM (or pure DMSO in case of the control). To determine the background fluorescence a sample without protein was prepared as well as a protein controls without inhibitor. The plate was measured on an I-cycler IQ single color real-time PCR (MyiQ™ iCycler, BioRad) system with an excitation wavelength of 490 nm and emission wavelength of 570 nm. The emission was monitored while the temperature was increased at 0.2 °C per 24 s (25 °C–79.80 °C). Data of the sEH-P measurements were analyzed by determining the maximum of first derivative curves given by MyIQ 1.0 software in Microsoft Excel after calculating the mean of the first derivative curves of the triplicate and data normalization. The temperature at the local maxima was assumed as the

melting point. For sEH-H samples the raw data was analyzed directly in GraphPad Prism (version 5.03; GraphPad Software, Inc.) using a Boltzmann sigmoidal fit. The V50 value of the fit was considered as the melting temperature. All samples were measured as triplicate on the plate as well as in three separate experiments. Statistical significance of the measured melting points in respect to the DMSO control was determined by a two-tailored T-test using GraphPad Prism (version 7.05; GraphPad Software, Inc.).

Isothermal titration calorimetry

ITC experiments were performed on a Nano ITC (TA Instruments, Waters GmbH) in inverse mode, with the protein solution in the 250 µL syringe, and the inhibitor sample in the 940 µL sample cell. Protein as well as inhibitor samples were prepared in assay buffer (50 mM acetate, 10 mM $MgCl_2$, 5% (v/v) Glycerol, pH 5.75) supplied with DMSO to a final concentration of 2%. The fresh protein solution used in the experiments had a fixed concentration of 185 µM. All measurements were performed at 25 °C with a stirring speed of 350 rpm. The number of titration steps (20-25) as well as the volume (8-10 µL) was adjusted according to the specific measurement. The delay between the injections was 200 s. All tested inhibitors have been prepared as 50 mM DMSO stock solutions. The inhibitor samples were prepared with the assay buffer adjusting the final DMSO concentration in the sample to 2% (v/v), while the concentration of inhibitor was chosen to optimize the shape of the curve. The gained data was analyzed using NanoAnalyze Data Analysis (version 3.5.0, TA Instruments).

Crystallization

The fresh sEH-P was concentrated to a concentration of 30 mg/ml before adding **22d** as 50 mM DMSO stock to a final amount of 2,08% (v/v) DMSO in the sample. After a 1h incubation on ice

the solution was centrifuged at max speed for 10 mins (4°C). The supernatant was used in 96 well screens (JCSG7) via sitting-drop vapor diffusion method mixing protein and reservoir buffer in three different ratios (50 nL +100 nL, 75 nL +75 nL, 100 nL +50 nL). Crystals appeared in the 20 °C screen after a few days in the well containing 25% (w/v) PEG3350, 0.1 M Bis-Tris pH 5.5 as reservoir buffer. The crystals were transferred into precipitant solution supplemented with 25% ethylenglycol for 1 min, before flash freezing in the liquid nitrogen. Diffraction of the crystals was checked in house at the SGC.

X-ray diffraction data of good diffracting crystals were collected at the beamline station I02 at the Diamond Light Source, Oxfordshire, England. All diffraction data were obtained from a single crystal and the data reduction was done with xia2[31] (0.4.0.291-ga780859-dials-1.1) while the scaling was done with SCALA[32,33]. The initial protein structure was determined at a resolution of 1.55 Å by molecular replacement with PHASER[34] program within PHENIX[35] software package using a truncated version of the full length sEH structure (pdb: 5ALU) were coordinates for heteroatoms (water and ligands) were excluded from the starting model.

After several iterative rounds of model building with COOT[36] into the 2Fo – Fc electron density map, the model containing polypeptide chain and the ligand was refined[37] to a final R_{word} and R_{free}-values of 0.2034 and 0.2305, respectively, using PHENIX software package[38] (version: 1.10.1_2155). The graphical representations were made using MOE (Chemical Computing Group, Montreal, Canada). Statistics of data collection and structural refinement were generated using the "Phenix table one" tool and are summarized in **Table 7**. The coordinates and structure-factor amplitudes have been deposited in the Protein Data Bank as entry 5MWA (**22d**).

Table 7. Data collection and refinement statistics.

Wavelength	0.979490
Resolution range	42.86 - 1.55 (1.605 - 1.55)
Space group	P 21 21 21
Unit cell	52.09 54.11 75.44 90 90 90
Total reflections	197971 (19739)
Unique reflections	31021 (1506)
Multiplicity	6.4 (6.6)
Completeness (%)	0.89 (0.48)
Mean I/sigma(I)	15.21 (2.68)
Wilson B-factor	14.31
R-merge	0.05117 (0.4581)
R-meas	0.05583 (0.4973)
CC1/2	0.999 (0.935)
CC*	1 (0.983)
Reflections used in refinement	28201 (1506)
Reflections used for R-free	1420 (90)
R-work	0.2034 (0.2306)
R-free	0.2305 (0.2527)
CC(work)	0.942 (0.853)
CC(free)	0.927 (0.800)
Number of non-hydrogen atoms	1766
macromolecules	1634
ligands	29

Protein residues	209
RMS(bonds)	0.014
RMS(angles)	1.23
Ramachandran favored (%)	98.52
Ramachandran allowed (%)	1.48
Ramachandran outliers (%)	0
Rotamer outliers (%)	0.56
Clashscore	2.98
Average B-factor	18.49
macromolecules	18.22
ligands	9.40
solvent	25.35

Statistics for the highest-resolution shell are shown in parentheses.

Cyclooxygenase assay

COX-1 and COX-2 inhibitory activity and selectivity have been carried out using human platelets and monocytes, respectively[39,40]. Briefly, washed human platelets, treated with increasing concentration of the tested compounds, were challenged with calcium ionophore A23187 in order to stimulate COX-1 dependent thromboxane A2 (TXA2) production. TXB2 (a stable TXA2 metabolite) was evaluated in the supernatant.

COX-2 activity was measured in monocytes resuspended in HBSS, in order to avoid compound binding to plasma-protein. COX-2 inhibition was evaluated quantifying prostaglandin E_2 (PGE2) production in LPS-challenged preparations pretreated with increasing concentration of the tested

compounds. PGE2 and thromboxane B2 (TXB2) concentrations were evaluated by liquid chromatography-tandem mass spectrometry using the isotopic dilution of the deuterated internal standards (IS) [d4]PGE2 and [d4]TXB2, as previously described[39]. Briefly, samples were spiked with IS and an aliquot injected into a liquid chromatograph Agilent 1100. Chromatography was carried out using a reverse phase eluted with a linear gradient from 25 to 100% solvent B (methanol:acetonitrile, 65:35) over 10 min (solvent A: 0.05% acetic acid pH 6 with ammonia). The effluent from the High-Performance Liquid Chromatography column was directly infused into an API4000 triple-quadrupole operated in negative ion mode, monitoring the following specific transitions: m/z 351>271 for PGE2, m/z 355>275 for [d4]PGE2, m/z 369>169 TXB2 and m/z 373>173 for [d4]TXB2. Quantitation has been carried out using standard curves obtained with synthetic standards.

Hybrid reporter gene assays for PPARα/γ/δ, LXRα/β, RXRα and FXR

Plasmids: The Gal4-fusion receptor plasmids pFA-CMV-hPPARα-LBD[41], pFA-CMV-hPPARγ-LBD[41], pFA-CMV-hPPARδ-LBD[41], pFA-CMV-hLXRα-LBD[42], pFA-CMV-hLXRβ-LBD[42], pFA-CMV-hRXRα-LBD[43] and pFA-CMV-hFXR-LBD coding for the hinge region and ligand binding domain (LBD) of the canonical isoform of the respective nuclear receptor have been reported previously. pFR-Luc (Stratagene) was used as reporter plasmid and pRL-SV40 (Promega) for normalization of transfection efficiency and cell growth.

Assay procedure: HEK293T cells were grown in DMEM high glucose, supplemented with 10% FCS, sodium pyruvate (1 mM), penicillin (100 U/ml) and streptomycin (100 µg/ml) at 37 °C and 5% CO_2. The day before transfection, HEK293T cells were seeded in 96-well plates ($2.5 \cdot 10^4$

cells/well). Before transfection, medium was changed to Opti-MEM without supplements. Transient transfection was carried out using Lipofectamine LTX reagent (Invitrogen) according to the manufacturer's protocol with pFR-Luc (Stratagene), pRL-SV40 (Promega) and pFA-CMV-hNR-LBD. 5 h after transfection, medium was changed to Opti-MEM supplemented with penicillin (100 U/ml), streptomycin (100 μg/ml), now additionally containing 0.1% DMSO and the respective test compound or 0.1% DMSO alone as untreated control. Each concentration was tested in triplicates and each experiment was repeated independently at least three times. Following overnight (12-14 h) incubation with the test compounds, cells were assayed for luciferase activity using Dual-Glo™ Luciferase Assay System (Promega) according to the manufacturer's protocol. Luminescence was measured with an Infinite M200 luminometer (Tecan Deutschland GmbH). Normalization of transfection efficiency and cell growth was done by division of firefly luciferase data by Renilla luciferase data and multiplying the value by 1000 resulting in relative light units (RLU). Fold activation was obtained by dividing the mean RLU of a test compound at a respective concentration by the mean RLU of untreated control. Relative activation was obtained by dividing the fold activation of a test compound at a respective concentration by the fold activation of a respective reference agonist at 1 μM (PPARα: GW7647; PPARγ: pioglitazone; PPARδ: L165,041; LXRα/β: T0901317; RXRα: bexarotene; FXR: GW4064). All hybrid assays were validated with the above-mentioned reference agonists which yielded EC_{50} values in agreement with literature.

AUTHOR INFORMATION

Corresponding Author

* E-mail: proschak@pharmchem.uni-frankfurt.de.

Author Contributions

The manuscript was written through contributions of all authors. All authors have given approval to the final version of the manuscript. ‡J.S.K and S.W. contributed equally.

Funding Sources

This work was supported by Deutsche Forschungsgemeinschaft (DFG; Sachbeihilfe PR1405/2-2; SFB 1039 Teilprojekt A07; Heisenberg-Professur PR1405/4-1) and by research funding programme Landes-Offensive zur Entwicklung Wissenschaftlich-ökonomischer Exzellenz (LOEWE) of the State of Hessen, Research Center for Translational Medicine and Pharmacology TMP). This work was supported in part by NIEHS grant ES02710 and NIEHS Superfund grant P42 ES04699. A.C. would like to acknowledge funding by the SFB autophagy. A.C. and S.K. are grateful for support by the German cancer network DKTK and the SGC, a registered charity (no. 1097737) that receives funds from AbbVie, Bayer Pharma AG, Boehringer Ingelheim, Canada Foundation for Innovation, Eshelman Institute for Innovation, Genome Canada through Ontario Genomics Institute [OGI-055], Innovative Medicines Initiative (EU/EFPIA) [ULTRA-DD grant no. 115766], Janssen, Merck KGaA, MSD, Novartis Pharma AG, Ontario Ministry of Research, Innovation and Science (MRIS), Pfizer, São Paulo Research Foundation-FAPESP, Takeda, and the Wellcome Trust. This work was co-supported in part for the in vivo study by the French National Research Agency (ANR-16-CE17-0012), European Union and Normandie Regional Council. Europe gets involved in Normandie with European Regional Development Fund (ERDF).

ACKNOWLEDGMENT

The crystal diffraction experiments were performed on Beamline station I02 at the Diamond Light Source, Oxfordshire, England. We thank Dr. F. J. Sorrell and Dr. N. Fox for assistance and support in using the beamline.

Accession Codes

Coordinates and structure factors are deposited at the Protein Data Bank with code 5MWA (**22d)**. The authors will release the atomic coordinates and experimental data upon article publication.

ABBREVIATIONS

BCA assay, bicinchoninic acid assay; CIU, *N*-cyclohexyl-*N*'-(4-iodophenyl)urea; COX-1, cyclooxygenase 1; COX-2; cyclooxygenase 2; CV, coefficient of variance; DMF, dimethylformamide; DSF, differential scanning fluorimetry; EETs, epoxyeicosatrienoic acids; EpFAs, epoxy fatty acids; FCS, fetal calf serum; FDP, fluorescein diphosphate; FXR, farnesoid X receptor; HTS, high-throughput screening; IS, internal standard; ITC, isothermal titration calorimetry; LBD, ligand binding domain; LDA, lithium diisopropylamide; LXR, Liver X receptor; NBS, n-bromosuccinimide; ORF, open reading frame; PGE2, prostaglandin E2, PPAR, peroxisome proliferator-activated receptor; RLU, relative light units; ROS, reactive oxygen species; RXR, retinoid X receptor; SAR, structure-activity relationships; SDS, sodium dodecyl sulfate; sEH, soluble epoxide hydrolase; sEH-H, C-terminal/hydrolase domain of the soluble epoxide hydrolase; sEHI, inhibitors of the C-terminal domain of sEH; sEH-P, N-terminal/phosphatase domain of the soluble epoxide hydrolase; TBAF, tetrabutyl ammonium fluoride solution; TCEP, tris(2-carboxyethyl)phosphine; TEV, tobacco etch virus; THF,

tetrahydrofuran; TMSCN, trimethylsilyl cyanide; TXA2, thromboxane A2; TXB2, thromboxane B2;

Supporting Information

The Supporting Information is available free of charge on the ACS Publication website at DOI:

- DSF experiments
- Experimental procedures of the performed animal experiments, including details about animals, surgery, treatment overview, sample collection, quantification of 22b, and determination of rat plasma levels of sEH substrates and metabolites
- PBMC experiments: results and experimental procedures
- Molecular formula strings (CSV)

REFERENCES

(1) Arand, M.; Cronin, A.; Oesch, F.; Mowbray, S. L.; Jones, T. A. The Telltale Structures of Epoxide Hydrolases. *Drug Metab. Rev.* **2003**, *35* (4), 365–383. https://doi.org/10.1081/DMR-120026498.

(2) Wagner, K. M.; McReynolds, C. B.; Schmidt, W. K.; Hammock, B. D. Soluble Epoxide Hydrolase as a Therapeutic Target for Pain, Inflammatory and Neurodegenerative Diseases. *Pharmacol. Ther.* **2017**, *180*, 62–76. https://doi.org/10.1016/j.pharmthera.2017.06.006.

(3) Inceoglu, B.; Bettaieb, A.; Haj, F. G.; Gomes, A. V.; Hammock, B. D. Modulation of Mitochondrial Dysfunction and Endoplasmic Reticulum Stress Are Key Mechanisms for the Wide-Ranging Actions of Epoxy Fatty Acids and Soluble Epoxide Hydrolase Inhibitors. *Prostaglandins Other Lipid Mediat.* **2017**, *133*, 68–78. https://doi.org/10.1016/j.prostaglandins.2017.08.003.

(4) Lazaar, A. L.; Yang, L.; Boardley, R. L.; Goyal, N. S.; Robertson, J.; Baldwin, S. J.; Newby, D. E.; Wilkinson, I. B.; Tal-Singer, R.; Mayer, R. J.; Cheriyan, J. Pharmacokinetics, Pharmacodynamics and Adverse Event Profile of GSK2256294, a Novel Soluble Epoxide Hydrolase Inhibitor. *Br J Clin Pharmacol* **2016**, *81* (5), 971–979. https://doi.org/10.1111/bcp.12855.

(5) Cronin, A.; Mowbray, S.; Dürk, H.; Homburg, S.; Fleming, I.; Fisslthaler, B.; Oesch, F.; Arand, M. The N-Terminal Domain of Mammalian Soluble Epoxide Hydrolase Is a Phosphatase. *Proc. Natl. Acad. Sci. U.S.A.* **2003**, *100* (4), 1552–1557. https://doi.org/10.1073/pnas.0437829100.

(6) Newman, J. W.; Morisseau, C.; Harris, T. R.; Hammock, B. D. The Soluble Epoxide Hydrolase Encoded by EPXH2 Is a Bifunctional Enzyme with Novel Lipid Phosphate Phosphatase Activity. *Proc. Natl. Acad. Sci. U.S.A.* **2003**, *100* (4), 1558–1563. https://doi.org/10.1073/pnas.0437724100.

(7) Tran, K. L.; Aronov, P. A.; Tanaka, H.; Newman, J. W.; Hammock, B. D.; Morisseau, C. Lipid Sulfates and Sulfonates Are Allosteric Competitive Inhibitors of the N-Terminal Phosphatase Activity of the Mammalian Soluble Epoxide Hydrolase. *Biochemistry* **2005**, *44* (36), 12179–12187. https://doi.org/10.1021/bi050842g.

(8) Morisseau, C.; Schebb, N. H.; Dong, H.; Ulu, A.; Aronov, P. A.; Hammock, B. D. Role of Soluble Epoxide Hydrolase Phosphatase Activity in the Metabolism of Lysophosphatidic Acids. *Biochem. Biophys. Res. Commun.* **2012**, *419* (4), 796–800. https://doi.org/10.1016/j.bbrc.2012.02.108.

(9) Oguro, A.; Imaoka, S. Lysophosphatidic Acids Are New Substrates for the Phosphatase Domain of Soluble Epoxide Hydrolase. *J. Lipid Res.* **2012**, *53* (3), 505–512. https://doi.org/10.1194/jlr.M022319.

(10) De Vivo, M.; Ensing, B.; Dal Peraro, M.; Gomez, G. A.; Christianson, D. W.; Klein, M. L. Proton Shuttles and Phosphatase Activity in Soluble Epoxide Hydrolase. *J. Am. Chem. Soc.* **2007**, *129* (2), 387–394. https://doi.org/10.1021/ja066150c.

(11) Kramer, J.; Proschak, E. Phosphatase Activity of Soluble Epoxide Hydrolase. *Prostaglandins & Other Lipid Mediators* **2017**, *133*, 88–92. https://doi.org/10.1016/j.prostaglandins.2017.07.002.

(12) Hou, H.-H.; Liao, Y.-J.; Hsiao, S.-H.; Shyue, S.-K.; Lee, T.-S. Role of Phosphatase Activity of Soluble Epoxide Hydrolase in Regulating Simvastatin-Activated Endothelial Nitric Oxide Synthase. *Sci Rep* **2015**, *5*, 13524. https://doi.org/10.1038/srep13524.

(13) Enayetallah, A. E.; Grant, D. F. Effects of Human Soluble Epoxide Hydrolase Polymorphisms on Isoprenoid Phosphate Hydrolysis. *Biochemical and Biophysical Research Communications* **2006**, *341* (1), 254–260. https://doi.org/10.1016/j.bbrc.2005.12.180.
(14) Matsumoto, N.; Suzuki, E.; Ishikawa, M.; Shirafuji, T.; Hasumi, K. Soluble Epoxide Hydrolase as an Anti-Inflammatory Target of the Thrombolytic Stroke Drug SMTP-7. *J. Biol. Chem.* **2014**, *289* (52), 35826–35838. https://doi.org/10.1074/jbc.M114.588087.
(15) Morisseau, C.; Sahdeo, S.; Cortopassi, G.; Hammock, B. D. Development of an HTS Assay for EPHX2 Phosphatase Activity and Screening of Nontargeted Libraries. *Anal. Biochem.* **2013**, *434* (1), 105–111. https://doi.org/10.1016/j.ab.2012.11.017.
(16) Klingler, F.-M.; Wolf, M.; Wittmann, S.; Gribbon, P.; Proschak, E. Bacterial Expression and HTS Assessment of Soluble Epoxide Hydrolase Phosphatase. *J Biomol Screen* **2016**, *21* (7), 689–694. https://doi.org/10.1177/1087057116637609.
(17) Stork, G.; Maldonado, L. Anions of Protected Cyanohydrins as Acyl Carbanion Equivalents and Their Use in a New Synthesis of Ketones. *J. Am. Chem. Soc.* **1971**, *93* (20), 5286–5287. https://doi.org/10.1021/ja00749a069.
(18) Topliss, J. G. Utilization of Operational Schemes for Analog Synthesis in Drug Design. *Journal of medicinal chemistry* **1972**, *15* (10), 1006–1011.
(19) Argiriadi, M. A.; Morisseau, C.; Goodrow, M. H.; Dowdy, D. L.; Hammock, B. D.; Christianson, D. W. Binding of Alkylurea Inhibitors to Epoxide Hydrolase Implicates Active Site Tyrosines in Substrate Activation. *J. Biol. Chem.* **2000**, *275* (20), 15265–15270. https://doi.org/10.1074/jbc.M000278200.
(20) Heroven, C.; Georgi, V.; Ganotra, G. K.; Brennan, P.; Wolfreys, F.; Wade, R. C.; Fernández-Montalván, A. E.; Chaikuad, A.; Knapp, S. Halogen-Aromatic π Interactions Modulate Inhibitor Residence Times. *Angew. Chem. Int. Ed. Engl.* **2018**, *57* (24), 7220–7224. https://doi.org/10.1002/anie.201801666.
(21) Falke, H.; Chaikuad, A.; Becker, A.; Loaëc, N.; Lozach, O.; Abu Jhaisha, S.; Becker, W.; Jones, P. G.; Preu, L.; Baumann, K.; Knapp, S.; Meijer, L.; Kunick, C. 10-Iodo-11H-Indolo[3,2-c]Quinoline-6-Carboxylic Acids Are Selective Inhibitors of DYRK1A. *J Med Chem* **2015**, *58* (7), 3131–3143. https://doi.org/10.1021/jm501994d.
(22) Öster, L.; Tapani, S.; Xue, Y.; Käck, H. Successful Generation of Structural Information for Fragment-Based Drug Discovery. *Drug Discov. Today* **2015**, *20* (9), 1104–1111. https://doi.org/10.1016/j.drudis.2015.04.005.
(23) Barbosa-Sicard, E.; Frömel, T.; Keserü, B.; Brandes, R. P.; Morisseau, C.; Hammock, B. D.; Braun, T.; Krüger, M.; Fleming, I. Inhibition of the Soluble Epoxide Hydrolase by Tyrosine Nitration. *J. Biol. Chem.* **2009**, *284* (41), 28156–28163. https://doi.org/10.1074/jbc.M109.054759.
(24) Hahn, S.; Achenbach, J.; Buscató, E.; Klingler, F.-M.; Schroeder, M.; Meirer, K.; Hieke, M.; Heering, J.; Barbosa-Sicard, E.; Loehr, F.; Fleming, I.; Doetsch, V.; Schubert-Zsilavecz, M.; Steinhilber, D.; Proschak, E. Complementary Screening Techniques Yielded Fragments That Inhibit the Phosphatase Activity of Soluble Epoxide Hydrolase. *ChemMedChem* **2011**, *6* (12), 2146–2149. https://doi.org/10.1002/cmdc.201100433.
(25) Lukin, A.; Kramer, J.; Hartmann, M.; Weizel, L.; Hernandez-Olmos, V.; Falahati, K.; Burghardt, I.; Kalinchenkova, N.; Bagnyukova, D.; Zhurilo, N.; Rautio. J.; Forsberg, M.; Ihalainen, J.; Auriola, S.; Leppänen, J.; Konstantinov, I.; Pogoryelov, D.; Proschak, E.; Dar'in, D.; Krasavin, M. Discovery of Polar Spirocyclic Orally Bioavailable Urea Inhibitors

of Soluble Epoxide Hydrolase. *Bioorg. Chem.* **2018**, *80*, 655–667. https://doi.org/10.1016/j.bioorg.2018.07.014.

(26) Studier, F. W. Protein Production by Auto-Induction in High Density Shaking Cultures. *Protein Expr. Purif.* **2005**, *41* (1), 207–234.

(27) Morisseau, C.; Beetham, J. K.; Pinot, F.; Debernard, S.; Newman, J. W.; Hammock, B. D. Cress and Potato Soluble Epoxide Hydrolases: Purification, Biochemical Characterization, and Comparison to Mammalian Enzymes. *Arch. Biochem. Biophys.* **2000**, *378* (2), 321–332. https://doi.org/10.1006/abbi.2000.1810.

(28) Morisseau, C.; Merzlikin, O.; Lin, A.; He, G.; Feng, W.; Padilla, I.; Denison, M. S.; Pessah, I. N.; Hammock, B. D. Toxicology in the Fast Lane: Application of High-Throughput Bioassays to Detect Modulation of Key Enzymes and Receptors. *Environ. Health Perspect.* **2009**, *117* (12), 1867–1872. https://doi.org/10.1289/ehp.0900834.

(29) Wolf, N. M.; Morisseau, C.; Jones, P. D.; Hock, B.; Hammock, B. D. Development of a High-Throughput Screen for Soluble Epoxide Hydrolase Inhibition. *Anal. Biochem.* **2006**, *355* (1), 71–80. https://doi.org/10.1016/j.ab.2006.04.045.

(30) Niesen, F. H.; Berglund, H.; Vedadi, M. The Use of Differential Scanning Fluorimetry to Detect Ligand Interactions That Promote Protein Stability. *Nat Protoc* **2007**, *2* (9), 2212–2221. https://doi.org/10.1038/nprot.2007.321.

(31) Winter, G.; Lobley, C. M. C.; Prince, S. M. Decision Making in Xia2. *Acta Crystallogr. D Biol. Crystallogr.* **2013**, *69* (Pt 7), 1260–1273. https://doi.org/10.1107/S0907444913015308.

(32) Winn, M. D.; Ballard, C. C.; Cowtan, K. D.; Dodson, E. J.; Emsley, P.; Evans, P. R.; Keegan, R. M.; Krissinel, E. B.; Leslie, A. G. W.; McCoy, A.; McNicholas, S.J.; Murshudov, G.N.; Pannu, N.S.; Potterton, E.A.; Powell, H.R.; Read, R.J.; Vagin, A.; Wilson, K.S. Overview of the CCP4 Suite and Current Developments. *Acta Crystallogr. D Biol. Crystallogr.* **2011**, *67* (Pt 4), 235–242. https://doi.org/10.1107/S0907444910045749.

(33) Evans, P. R. An Introduction to Data Reduction: Space-Group Determination, Scaling and Intensity Statistics. *Acta Crystallogr. D Biol. Crystallogr.* **2011**, *67* (Pt 4), 282–292. https://doi.org/10.1107/S090744491003982X.

(34) McCoy, A. J.; Grosse-Kunstleve, R. W.; Adams, P. D.; Winn, M. D.; Storoni, L. C.; Read, R. J. Phaser Crystallographic Software. *J Appl Crystallogr* **2007**, *40* (Pt 4), 658–674. https://doi.org/10.1107/S0021889807021206.

(35) Adams, P. D.; Afonine, P. V.; Bunkóczi, G.; Chen, V. B.; Davis, I. W.; Echols, N.; Headd, J. J.; Hung, L.-W.; Kapral, G. J.; Grosse-Kunstleve, R. W.; McCoy, A.J.; Moriarty, N.W.; Oeffner, R.; Read, R.J.; Richardson, D.C.; Richardson, J.S.; Terwilliger, T.C.; Zwart, P.H. PHENIX: A Comprehensive Python-Based System for Macromolecular Structure Solution. *Acta Crystallogr. D Biol. Crystallogr.* **2010**, *66* (Pt 2), 213–221. https://doi.org/10.1107/S0907444909052925.

(36) Emsley, P.; Lohkamp, B.; Scott, W. G.; Cowtan, K. Features and Development of Coot. *Acta Crystallogr. D Biol. Crystallogr.* **2010**, *66* (Pt 4), 486–501. https://doi.org/10.1107/S0907444910007493.

(37) Moriarty, N. W.; Grosse-Kunstleve, R. W.; Adams, P. D. Electronic Ligand Builder and Optimization Workbench (ELBOW): A Tool for Ligand Coordinate and Restraint Generation. *Acta Crystallogr. D Biol. Crystallogr.* **2009**, *65* (Pt 10), 1074–1080. https://doi.org/10.1107/S0907444909029436.

(38) Afonine, P. V.; Grosse-Kunstleve, R. W.; Echols, N.; Headd, J. J.; Moriarty, N. W.; Mustyakimov, M.; Terwilliger, T. C.; Urzhumtsev, A.; Zwart, P. H.; Adams, P. D. Towards

Automated Crystallographic Structure Refinement with Phenix.Refine. *Acta Crystallogr. D Biol. Crystallogr.* **2012**, *68* (Pt 4), 352–367. https://doi.org/10.1107/S0907444912001308.

(39) Hoxha, M.; Buccellati, C.; Capra, V.; Garella, D.; Cena, C.; Rolando, B.; Fruttero, R.; Carnevali, S.; Sala, A.; Rovati, G. E.; Bertinaria, M. In Vitro Pharmacological Evaluation of Multitarget Agents for Thromboxane Prostanoid Receptor Antagonism and COX-2 Inhibition. *Pharmacol. Res.* **2016**, *103*, 132–143. https://doi.org/10.1016/j.phrs.2015.11.012.

(40) Bertinaria, M.; Shaikh, M. A. A. G.; Buccellati, C.; Cena, C.; Rolando, B.; Lazzarato, L.; Fruttero, R.; Gasco, A.; Hoxha, M.; Capra, V.; Sala, A.; Rovati, G.E. Designing Multitarget Anti-Inflammatory Agents: Chemical Modulation of the Lumiracoxib Structure toward Dual Thromboxane Antagonists-COX-2 Inhibitors. *ChemMedChem* **2012**, *7* (9), 1647–1660. https://doi.org/10.1002/cmdc.201200272.

(41) Rau, O.; Wurglics, M.; Paulke, A.; Zitzkowski, J.; Meindl, N.; Bock, A.; Dingermann, T.; Abdel-Tawab, M.; Schubert-Zsilavecz, M. Carnosic Acid and Carnosol, Phenolic Diterpene Compounds of the Labiate Herbs Rosemary and Sage, Are Activators of the Human Peroxisome Proliferator-Activated Receptor Gamma. *Planta Med.* **2006**, *72* (10), 881–887. https://doi.org/10.1055/s-2006-946680.

(42) Heitel, P.; Achenbach, J.; Moser, D.; Proschak, E.; Merk, D. DrugBank Screening Revealed Alitretinoin and Bexarotene as Liver X Receptor Modulators. *Bioorg. Med. Chem. Lett.* **2017**, *27* (5), 1193–1198. https://doi.org/10.1016/j.bmcl.2017.01.066.

(43) Flesch, D.; Cheung, S.-Y.; Schmidt, J.; Gabler, M.; Heitel, P.; Kramer, J.; Kaiser, A.; Hartmann, M.; Lindner, M.; Lüddens-Dämgen, K.; Heering, J.; Lamers, C.; Lüddens, H.; Wurglics, M.; Proschak, E.; Schubert-Zsilavecz, M.; Merk, D. Nonacidic Farnesoid X Receptor Modulators. *J. Med. Chem.* **2017**, *60* (16), 7199–7205. https://doi.org/10.1021/acs.jmedchem.7b00903.

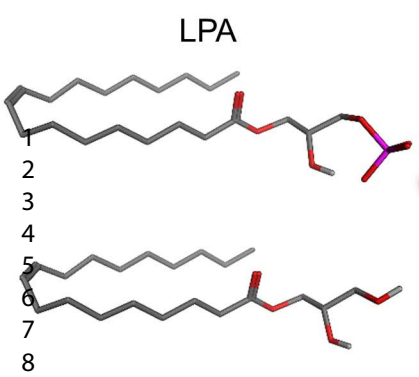

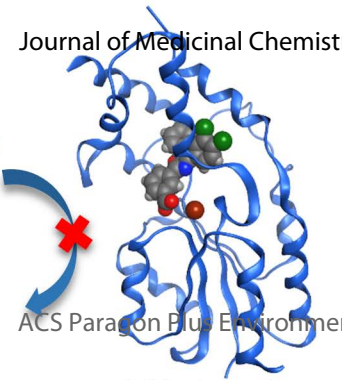

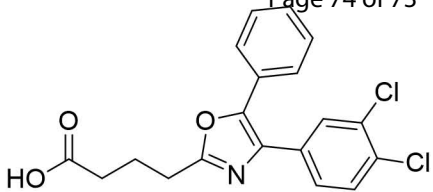

SWE101

IC_{50}(sEH-P) = 0.058 μM

active in vivo